Dysregulation of *Npas4* and *Inhba* expression and an altered excitation–inhibition balance are associated with cognitive deficits in DBA/2 mice

Kristin Oberländer,[1] Victoria Witte,[1] Anne Stephanie Mallien,[2] Peter Gass,[2] C. Peter Bengtson,[1] and Hilmar Bading[1]

[1]Department of Neurobiology, Interdisciplinary Center for Neurosciences (IZN), Heidelberg University, 69120 Heidelberg, Germany; [2]Department of Psychiatry and Psychotherapy, Research Group Animal Models in Psychiatry, Central Institute of Mental Health, Medical Faculty Mannheim/Heidelberg University, 68159 Mannheim, Germany

Differences in the learning associated transcriptional profiles between mouse strains with distinct learning abilities could provide insight into the molecular basis of learning and memory. The inbred mouse strain DBA/2 shows deficits in hippocampus-dependent memory, yet the transcriptional responses to learning and the underlying mechanisms of the impairments are unknown. Comparing DBA/2J mice with the reference standard C57BL/6N mouse strain we verify an enhanced susceptibility to kainic acid induced seizures, confirm impairments in hippocampus-dependent spatial memory tasks and uncover additional behavioral abnormalities including deficits in hippocampus-independent learning. Surprisingly, we found no broad dysfunction of the DBA/2J strain in immediate early gene (IEG) activation but instead report brain region-specific and gene-specific alterations. The learning-associated IEGs *Arc*, *c-Fos*, and *Nr4a1* showed no DBA/2J deficits in basal or synaptic activity induced gene expression in hippocampal or cortical primary neuronal cultures or in the CA1, CA3, or retrosplenial cortex following spatial object recognition (SOR) training in vivo. However, the parietal cortex showed reduced and the dentate gyrus showed enhanced SOR-evoked induction of most IEGs. All DBA/2J hippocampal regions exhibited elevated basal expression of inhibin β A (*Inhba*) and a learning-associated superinduction of the transcription factor neuronal Per-Arnt-Sim domain protein 4 (*Npas4*) known to regulate the synaptic excitation–inhibition balance. In line with this, CA1 pyramidal neurons of DBA/2J mice showed fewer inhibitory and more excitatory miniature postsynaptic currents but no alteration in most other electrophysiological properties or gross dendritic morphology. The dysregulation of *Npas4* and *Inhba* expression and synaptic connectivity may underlie the cognitive deficits and increased susceptibility to seizures of DBA/2J mice.

Inbred mouse strains carry naturally occurring genotypes not generated by artificial gene modifications and thus have the potential to provide insight into the molecular, cellular, and structural causes of interindividual differences attributable to genetic variants in humans. DBA mice are the oldest inbred strain that shows several strain-specific differences to the most widely used inbred strain, C57BL/6, including an increased susceptibility to hearing loss, noise-induced seizures, and glaucoma (Schreiber and Graham 1976; Willott and Lu 1980; Reichstein et al. 2007; Seo et al. 2021). Behaviorally, DBA/2 show hyperactivity (Thinus-Blanc et al. 1996; Podhorna and Brown 2002), impaired novelty induced locomotor activity and impaired hippocampus-dependent spatial learning in tasks such as contextual fear conditioning (CFC) (Paylor et al. 1994; Cabib et al. 2002; Tipps et al. 2014), the Morris water maze (Upchurch and Wehner 1988; Paylor et al. 1993; Logue et al. 1997; Owen et al. 1997; Nguyen et al. 2000a; Holmes et al. 2002; Youn et al. 2012), the eight-arm radial maze (Rossi-Arnaud et al. 1991) and object–place recognition (also termed spatial object recognition [SOR]) (Thinus-Blanc et al. 1996). In contrast, DBA/2 mice do not differ from C57BL/6 mice in several tasks that are largely independent of hippocampal function such as auditory fear conditioning (Paylor et al. 1994), passive avoidance (Podhorna and Brown 2002), conditioned taste aversion (Rebecca Glatt et al. 2016) and novel object recognition (Brooks et al. 2005; but see Thinus-Blanc et al. 1996).

Hippocampal connectivity, morphology and signal transduction, particularly in CA1 pyramidal neurons, play a major role in spatial memory acquisition (Volpe et al. 1992). Morphological features including the apical dendrite length and spine density of CA1 pyramidal neurons appear not to differ between DBA/2 and C57BL/6 mouse strains (Restivo et al. 2006). However, deficits in presynaptic vesicle release proteins, a reduced synaptic vesicle reserve pool and release probability at CA1 synapses without altered postsynaptic density or active zone sizes have been reported in DBA/2 mice (Nguyen et al. 2000a; Lenselink et al. 2015). Furthermore, synaptic dysfunction in DBA/2 mice is evident from a reduced mossy fiber terminal field in the CA3 (Crusio and Schwegler 1987) and impaired long-term potentiation (LTP) induction and/or maintenance in acute slices and in vivo in the CA1 (Matsuyama et al. 1997; Nguyen et al. 2000a,b; Jones et al. 2001; Gerlai 2002; Schimanski and Nguyen 2005) and dentate gyrus

Corresponding authors: bengtson@nbio.uni-heidelberg.de, bading@nbio.uni-heidelberg.de

(Bampton et al. 1999; Jones et al. 2001). DBA/2 mice also show lower levels of protein kinase C activity in their hippocampus and impaired learning induced phosphorylation of its target, GAP-43 (Wehner et al. 1990; Young et al. 2000; Jones et al. 2001). Thus, a synaptic dysfunction exists in the hippocampus of DBA/2 mice, yet little is known about the strain-dependent differences between DBA/2 and C57BL/6 at a molecular level in the context of hippocampus-dependent learning.

N-methyl-D-aspartate (NMDA) receptor-dependent signaling, which is important for the induction of immediate early genes (IEGs), is a well characterized and essential pathway involved in learning and memory (Bading et al. 1993; Tsien et al. 1996; Guzowski et al. 2001; Bading 2013). IEG induction is also an important and measurable endpoint of the NMDA receptor-dependent calcium signaling cascade. Memory impairments result from knockdown or knockout of IEGs such as *Nr4a1* (Hawk et al. 2012; Bridi and Abel 2013) and *Npas4* (Sun and Lin 2016; Weng et al. 2018) or transcription-regulating factors that mediate IEG induction such as cAMP response element binding protein (CREB) binding protein (CBP) and extracellular signal-regulated kinase 2 (ERK2) (Satoh et al. 2007; Barrett et al. 2011). CREB phosphorylation in response to hippocampal-dependent place learning or fear conditioning is reduced in the hippocampus of DBA/2 mice (Sung et al. 2008; Hwang et al. 2010; Cho et al. 2019) suggesting impaired learning related transcriptional activation.

Although IEGs are important for long-term memory formation, and gene expression in DBA/2 has been investigated in other contexts such as stress or physical activity (e.g., Fordyce et al. 1994; Mozhui et al. 2010; Misiewicz et al. 2019), little is known about IEG expression or induction by learning paradigms in DBA/2 mice. One study of spatial learning-induced expression of the IEG, *c-Fos*, in DBA/2 compared with C57BL/6 mice has reported time point- and subregion-specific differences between strains in the hippocampus (Passino et al. 2002). It remains to be seen whether other IEGs follow this expression profile.

The central aim of this study was to deepen our knowledge of the molecular, structural, and cellular properties associated with strain-dependent differences in learning in mice. Specifically, we asked whether impaired hippocampus-dependent spatial memory in DBA/2J mice is accompanied by altered IEG basal expression and/or induction by relevant learning paradigms. We first verified hippocampus-dependent learning impairment and long-term memory deficit in DBA/2J mice independent of confounding anxiety differences. We also investigated whether memory impairment is restricted to hippocampus-specific tasks. At a cellular level, we analyzed basic morphological and electrophysiological properties of CA1 pyramidal neurons including their synaptic connectivity and excitability. Finally, IEG expression was analyzed in vitro to investigate intrinsic network activity and signaling in primary hippocampal and cortical cultures, and in vivo to assess behaviorally induced gene expression in multiple brain regions. Our results confirm spatial memory deficits in DBA/2J mice accompanied by altered expression of *Inhba* and *Npas4*, two IEGs involved in regulating synaptic connectivity (Lin et al. 2008; Krieglstein et al. 2011). We further show a shift in the excitation–inhibition balance of synaptic transmission in DBA/2J mice as well as hyperactivity, anxiety-like behavior, and an increased susceptibility to seizures.

Results

DBA/2J learning deficits include but are not restricted to hippocampus-dependent tasks

Since protocols assessing memory performance vary between laboratories and even minor differences can influence behavioral performance, we first verified the DBA/2J spatial memory impairment with our CFC and SOR protocols. To minimize hormonal influences and to investigate strain differences independent of any developmental differences, we used 3-mo-old (young adult) males. We assessed both short-term and long-term memory (STM and LTM) for spatial learning and compared the performance of DBA/2J with that of the control inbred strain C57BL/6N. In line with previous reports, we found that DBA/2J show a severe impairment in CFC evidenced by a reduced freezing time compared with C57BL/6N mice during the test phase for both STM and LTM assessed 1 and 24 h after training, respectively (STM: $t_{(44)} = 11$, $P < 0.0001$; LTM: $t_{(44)} = 11.27$, $P < 0.0001$) (Fig. 1A). In addition, DBA/2J mice displayed increased sensitivity to the shock shown by an elevated velocity of movement during the shock ($t_{(84)} = 5.04$, $P < 0.0001$) (Fig. 1B, left) followed by increased proportion of time spent freezing (postshock freezing; DBA/2: $t_{(48)} = 4.469$, $P < 0.0001$) (Fig. 1C, right). This is in line with a previous report showing elevated freezing immediately after shock application in DBA/2 compared with C57BL/6 (Gerlai 1998) and indicates that the reduced freezing time in DBA/2J during the test phase is not caused by a reduced pain perception during training or any impaired ability of DBA/2J mice to freeze. Although CFC is considered a hippocampus-dependent memory paradigm, amygdala-dependent anxiety and fear also influence CFC performance (Kochli et al. 2015). We observed increased anxiety-like behavior in an open field task in DBA/2J compared with C57BL/6N for several parameters (number of entries in central zone, $t_{(44)} = 4.191$, $P < 0.0001$; latency to first entry into the central zone, $t_{(43)} = 2.991$, $P = 0.0046$; time spent in central zone, $t_{(44)} = 2.629$, $P = 0.0118$) (Fig. 1D). Increased anxiety in DBA/2J mice could potentially interfere with learning in the CFC task and reduce their performance. To verify the hippocampal memory deficit independent of anxiety confound, we analyzed DBA/2J performance in SOR, a hippocampus-dependent memory task that assesses the exploration time of a relocated object during the test phase and does not evoke significant anxiety or involve an aversive stimulus. In this task, DBA/2J mice showed a significant impairment in LTM ($t_{(26)} = 2.490$, $P = 0.0195$) but not STM ($t_{(19)} = 1.136$, $P = 0.2699$), indicating a specific deficit in hippocampus-dependent LTM formation (Fig. 1E). Two further parameters indicative of hippocampal dysfunction were observed in DBA/2J mice: increased exploration in a novel environment ($F_{(1,48)} = 65.48$, $P < 0.0001$) (Fig. 1F) and impaired nesting behavior (mass of untorn nesting material DBA/2J: $t_{(18)} = 9.467$, $P < 0.0001$) (Fig. 1G), which have been reported to occur in hippocampus-lesioned mice and rats (Nadel 1968; Deacon 2006).

To assess the selectivity of DBA/2J memory impairment for hippocampus-dependent tasks we used a visuomotor conditional learning (VMCL) task, which is hippocampus-independent and relies predominantly on striatal and posterior cingulate cortex function (Horner et al. 2013; Delotterie et al. 2015). We used a Bussey–Saskida touch screen chamber for rodents (Horner et al. 2013) where food restricted mice were rewarded with milk if they learned to associate a symbol with a side-specific touch response following repeated paired presentations. DBA/2J mice showed a severe learning impairment in this task as indicated by lower accuracy ($F_{(14,285)} = 12.51$, $P < 0.0001$) and a higher number of correction trials ($F_{(19,380)} = 41.22$, $P < 0.0001$) (Fig. 1H). Thus, the learning impairment of DBA/2J mice seems not to exclusively affect hippocampus-dependent tasks. Since SOR, exploration, nest building and VMCL all rely on processing and coordination in and between the visual and motor systems, we next tested the visuospatial function in a visual water maze task. This task required mice to find a submerged but visible platform over four trials and is distinct from the standard Morris water maze task, which tests hippocampus-dependent spatial memory where the platform is not visible to the mouse in the test phase. DBA/2J and C57BL/6N mice
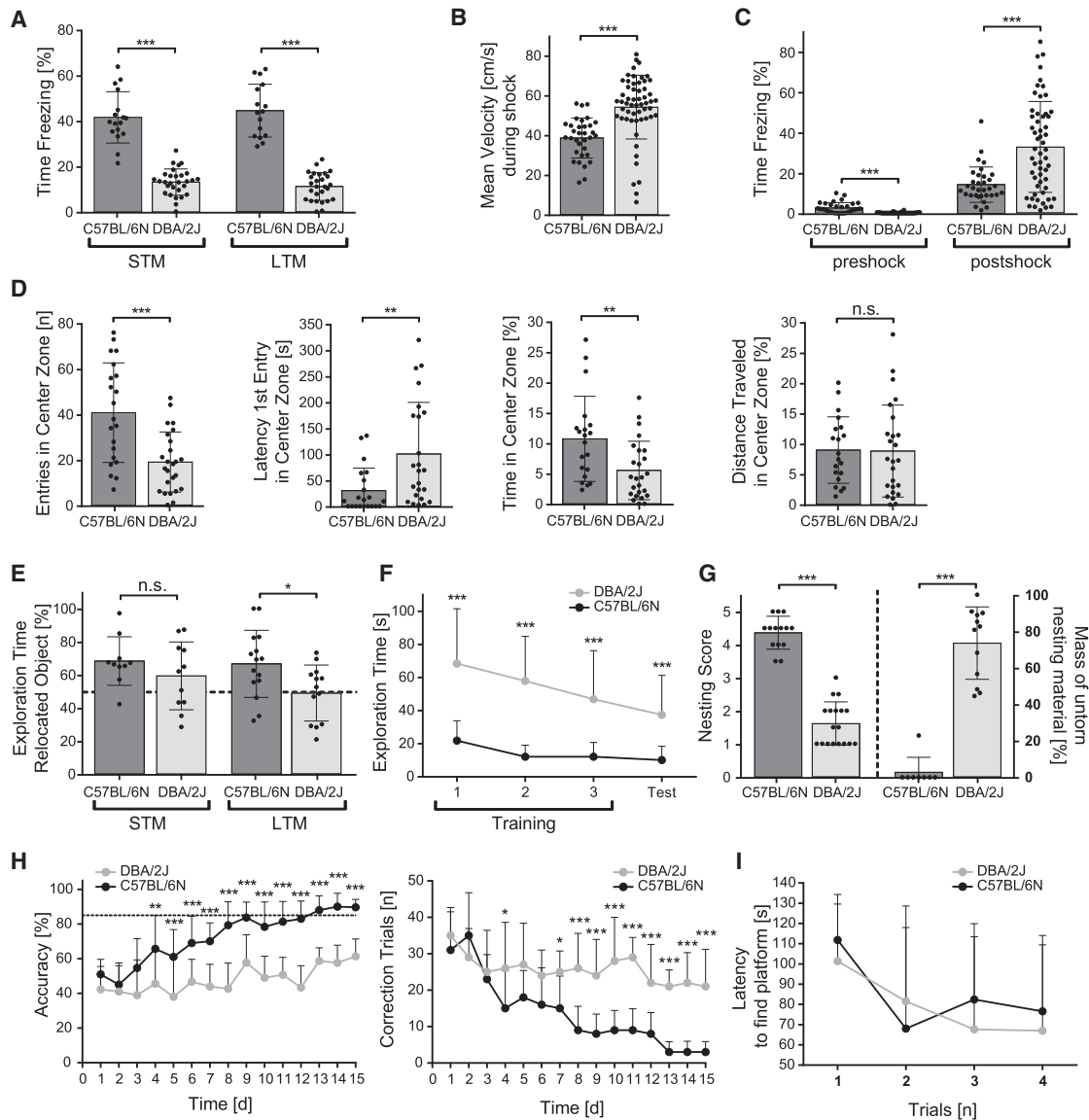
Figure 1. Comparison of DBA/2J and C57BL/6N learning and behavior. (*A*) CFC memory performance quantified as the time spent freezing as a percentage of total time during the test sessions for STM and LTM. Number of mice: C57BL/6N, STM $n = 17$; DBA/2J, STM $n = 29$; C57BL/6N, LTM $n = 16$; DBA/2J, LTM $n = 27$. (*B*) Mean velocity of mouse movement within the arena during the shock used as the unconditioned stimulus during CFC training (0.7 mA shock for 5 sec). (*C*) Time freezing as a percentage of the total time during the preshock and postshock periods (148 and 30 sec, respectively). Number of mice: C57BL/6N $n = 33$; DBA/2J $n = 56$. (*D*) Anxiety parameters quantified from the open field test. Number of mice: C57BL/6N $n = 21$; DBA/2J $n = 25$. (*E*) SOR memory performance quantified as the time spent exploring the relocated object as a percentage of the total exploration time during the test session. Number of mice: C57BL/6N, STM $n = 10$; DBA/2J, STM $n = 11$; C57BL/6N, LTM $n = 15$; DBA/2J, LTM $n = 13$. For both spatial memory tests (CFC and SOR) STM was tested 1 h and LTM 24 h after the training session. (*F*) The total object exploration time during all SOR training and test sessions is plotted. Number of mice: C57BL/6N $n = 29$; DBA/2J $n = 21$. (*G*) Nesting score evaluated according to Deacon (2006) (see the Materials and Methods) is plotted at the *left*. The mass of untorn cotton nesting material after 12 h as a percentage of the mass of total material placed in the cage is plotted at the *right*. Number of mice: C57BL/6N $n = 14$; DBA/2J $n = 12$. (*H, left*) Visuomotor conditional learning (VMCL) learning performance scored as the number of correct responses as percentage of the total number of responses over 15 d. (*Right*) VMCL learning performance is plotted as the number of correction trials after an incorrect response. Number of mice: C57BL/6N $n = 10$; DBA/2J $n = 10$. (*I*) Latency to find the visible platform during four trials of a water maze task. Number of mice: C57BL/6N $n = 5$; DBA/2J $n = 11$. All graphs are plotted as mean ± SD. Statistical significance was determined by independent, two-tailed *t*-test (*A–E, G*) and multiple-comparison two-way ANOVA (*F,H,I*). (n.s.) Not significant, (*) $P < 0.05$, (**) $P < 0.01$, (***) $P < 0.001$.

performed equally well in this task indicating no visuomotor impairment ($F_{(1,56)} = 0.2214$, $P = 0.6398$) (Fig. 1I). Taken together, our behavioral analyses are in line with previous studies showing impaired hippocampus-dependent memory function in DBA/2 mice. They further revealed that these deficits are independent of confounding differences in anxiety or visuomotor abilities and are not restricted to hippocampus-dependent tasks.

Strain differences in the morphology and electrophysiological passive cell properties of pyramidal CA1 neurons

Considering the severe spatial memory impairments of DBA/2J mice, we next analyzed hippocampal structure and basic electrophysiological parameters of CA1 pyramidal neurons, which could

underlie a strain-dependent behavioral impairment. Consistent with previous studies (Abusaad et al. 1999), cresyl violet staining did not reveal any obvious strain differences in gross hippocampal morphology (Fig. 2A). To investigate morphological properties in more detail, we measured total dendritic length of basal dendrites of Golgi-Cox-stained CA1 pyramidal neurons. CA1 excitatory neurons were chosen because of their well-documented role in spatial memory formation (Tsien et al. 1996; Hemstedt et al. 2017). In DBA/2J mice, there was a small but not statistically significant reduction in basal dendrite length ($t_{(35)} = 1.944$, $P = 0.0599$) (Fig. 2B), indicating that there may be a minor morphological impairment in the hippocampus of DBA/2J mice.

We performed whole-cell patch clamp recordings of CA1 pyramidal neurons in acute hippocampal slices to investigate potential differences in various electrophysiological properties between DBA/2J and C57BL/6N mice (Table 1). Major factors such as cell size, morphology and channel activity at rest that influence neuronal function affect passive electrophysiological properties. No differences were detected in whole-cell resistance and resting membrane potential, but a larger whole-cell capacitance was found in DBA/2J cells. We also compared various action potential (AP) parameters to detect any difference in excitability but found no difference in AP threshold, amplitude, half-width or rheobase current, the minimal current injection required to evoke an AP (Ta-

ble 1). DBA/2J cells showed a larger afterhyperpolarization potential (AHP) amplitude without significant differences in the delay to its peak. A larger AHP might be expected to reduce spike numbers and increase accommodation within spike trains. However, the number of APs evoked by incremental current steps did not differ between the mouse strains (Fig. 2C,D), and the slowing of AP frequency across these 1-sec depolarizing steps, quantified as an accommodation index, did not differ either (Table 1). Hyperpolarization-activated cyclic nucleotide-gated (HCN) cationic channels, responsible for the h current, and rapidly activating potassium inward rectifier (Kir) channels are known to regulate dendritic excitability and resting membrane potential in pyramidal neurons (Poolos et al. 2002; Day et al. 2005; Kase and Imoto 2012). We found no differences in these hyperpolarization-activated conductances, HCN, and Kir, between mouse strains. Thus, we detected no differences in passive electrical properties, excitability, AP firing frequency or hyperpolarization-activated conductances, except a slightly elevated whole-cell capacitance and AHP amplitude in CA1 pyramidal neurons of DBA/2J mice. The larger capacitance of DBA/2J CA1 pyramidal neurons suggests a large plasma membrane surface area indicative of a larger dendritic tree. Given the absence of any difference in the total dendrite lengths in the basal dendritic tree, such differences may arise from the larger apical dendritic tree that is too large for analysis with light microscopy. Taken together, we could not detect major morphological or electrophysiological differences of CA1 pyramidal neurons between DBA/2J and C57BL/6N mouse strains, suggesting that the severe learning impairments in DBA/2J mice are not caused by basal differences in the anatomy or electrical function of individual neurons but instead by deficits in gene expression or network function underlying adaptive responses.

Figure 2. Comparative analysis of DBA/2J and C57BL/6N hippocampal and dendritic morphology. (A) Representative pictures of C57BL/6N (left) and DBA/2J (right) dorsal and ventral hippocampus stained by cresyl violet (Nissl). (CA1) cornu ammonis area 1, (CA3) cornu ammonis area 3, (DG) dentate gyrus. Magnification, 10×. (B) Total dendritic length of basal dendrites of CA1 pyramidal neurons. Length was determined after manual tracing of Golgi-stained brain slices. C57BL/6N $n = 17$ cells, three animals; DBA/2J $n = 20$ cells, three animals. Statistical significance was determined by independent, two-tailed t-test. (C) The graph shows mean (±SEM) number of action potentials (APs) generated in response to a 1-sec current injection through the patch pipette with the cell at its resting membrane potential (V_{rest}; i.e., no holding current) from CA1 pyramidal neurons in C57BL/6N ($n = 21$) and DBA/2J ($n = 23$) mice. (D) The graph shows the same data set shown in C but with rheobase current (see Table 1) subtracted from all current injection values to adjust the data for any differences in rheobase current between cells. No significant differences occurred between the C57BL/6N and DBA/2J data sets for either analysis (independent samples t-tests of the slopes generated from linear fits for each cell: $t_{(44)} = 0.859$, $P = 0.395$ for C, and $t_{(44)} = 1.255$, $P = 0.217$ for D).

Comparative analysis of IEG induction in DBA/2J and C57BL/6N mice

Since no major strain differences in basic morphology and electrophysiology were apparent in CA1, we reasoned that either molecular signaling or hippocampal network functions might be compromised in the DBA/2J strain. The disruption of LTM but not STM in DBA/2J mice in SOR suggests impaired transcriptional responses to synaptic activity in the hippocampus. To assess synaptic activity induced IEG activation independent of in vivo network activity we examined IEG induction in primary hippocampal cultures from C57BL/6N and DBA/2J mice stimulated with bicuculline. This γ-aminobutyric acid type A (GABA$_A$) receptor antagonist causes AP bursting, synaptic NMDA receptor activation, synaptic potentiation, and calcium-dependent signaling cascades, leading to the induction of a large gene pool, including multiple IEGs (Hardingham et al. 2001; Arnold et al. 2005; Zhang et al. 2007, 2009). We quantified the induction strength and kinetics of three well-characterized NMDA receptor signaling-dependent IEGs: *Arc*,
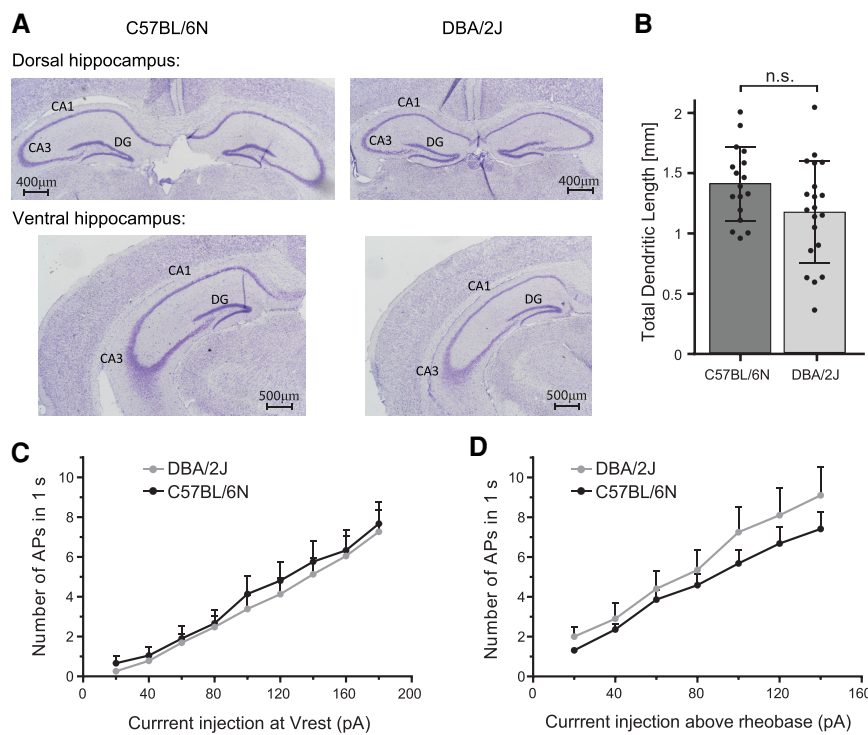
Table 1. Electrophysiological properties of CA1 pyramidal neurons in C57BL/6N or DBA/2J mice

		C57BL/6N	DBA/2J	*t*-value	*P*-value
Membrane capacitance	pF	124.9 ± 3.9 (78, 22)	137.3 ± 4.5 (85, 28)	2.06	0.040*
Membrane resistance	MΩ	131.8 ± 4.4 (78, 22)	135.4 ± 4.9 (85, 28)	0.53	0.594
V_{rest}	mV	−60.19 ± 0.74 (26, 8)	−58.33 ± 1.20 (28, 8)	1.29	0.201
AP threshold	mV	−40.22 ± 1.16 (26, 8)	−37.57 ± 1.35 (28, 8)	1.48	0.145
AP amplitude	mV	72.10 ± 2.02 (26, 8)	70.19 ± 2.38 (28, 8)	0.61	0.546
AP half width	msec	0.923 ± 0.028 (26, 8)	0.896 ± 0.032 (28, 8)	0.63	0.530
AHP amplitude	mV	−15.86 ± 0.90 (26, 8)	−18.69 ± 0.67 (28, 8)	2.54	0.014*
AHP peak delay	msec	4.58 ± 0.54 (26, 8)	4.99 ± 0.62 (28, 8)	0.48	0.631
Rheobase current	pA	58.5 ± 9.1 (27, 8)	61.3 ± 8.4 (30, 8)	0.23	0.820
Accommodation index	a.u.	0.40 ± 0.03 (25, 8)	0.44 ± 0.02 (28, 8)	1.34	0.187
Kir conductance	nS	2.90 ± 0.41 (25, 8)	3.08 ± 0.42 (28, 8)	0.31	0.757
HCN conductance	nS	2.73 ± 0.27 (25, 8)	2.95 ± 0.19 (28, 8)	0.69	0.494
mIPSC IEI	msec	91.05 ± 4.96 (21, 6)	136.51 ± 12.28 (20, 5)	3.49	0.0012**
mIPSC amplitude	pA	46.83 ± 2.72 (21,6)	54.05 ± 2.68 (20, 5)	1.89	0.066
mEPSC IEI	msec	3516 ± 282 (26, 10)	2663 ± 189 (35, 11)	2.61	0.0115*
mEPSC amplitude	pA	10.76 ± 0.32 (26, 10)	10.24 ± 0.30 (35, 11)	1.17	0.246

Summary statistics obtained from whole-cell patch-clamp recordings in acute hippocampal slices from 10-wk-old mice. Data indicate mean ± SEM (number of cells, number of animals). See the Materials and Methods for details. (V_{rest}) Resting membrane potential, (AP) action potential, (AHP) afterhyperpolarization potential, (HCN) hyperpolarization-activated cyclic nucleotide-regulated, (Kir) potassium inward rectifier, (mIPSC) miniature inhibitory postsynaptic current, (mEPSC) miniature excitatory postsynaptic current, (IEI) interevent interval. (*) $P < 0.05$, (**) $P < 0.01$ determined by two-tailed *t*-tests.

Npas4, and *Nr4a1*. Basal IEG expression and AP bursting-induced IEG induction were equivalent in hippocampal cultures prepared from DBA/2J and C57BL/6N mice (Fig. 3A). We performed the same analysis in primary cortical cultures to sample another brain region and found significantly higher activation of *Npas4* by bicuculline in DBA/2J cultures and a trend for elevated induction of *Arc* and *Nr4a1* (Fig. 3B). These results indicate that NMDA receptor and calcium signaling-dependent IEG induction pathways are not dysfunctional in DBA/2J neurons and that the machinery for the synaptic activation of transcription relevant to synaptic plasticity appears intact in culture systems of primary hippocampal and cortical neurons with some evidence for enhanced IEG activation in cortical preparations from DBA/2J mice.

To analyze IEG induction in the intact brain, we induced synaptic activity by a systemic injection of kainic acid. Kainate receptors are highly expressed in hippocampal regions (Wisden and Seeburg 1993) and their activation results in excitatory signaling- and activity-dependent gene induction, accompanied by convulsive seizures (status epilepticus) in a dose-dependent manner (Gall et al. 1991). DBA/2J mice showed higher status epilepticus scores ($t_{(17)} = 4.96$, $P < 0.0001$) (Fig. 4A) and even low kainic acid concentrations of 15 mg/kg body weight, which had little effect on C57BL/6N mice, were lethal for more than 50% of DBA/2J mice (Fig. 4B). Increased seizure susceptibility in DBA/2J has been reported for sound-induced seizures (Schreiber and Graham 1976). The extreme difference in seizure severity and lethality between the strains invalidated any meaningful comparison of kainic acid-induced gene induction (data not shown). Temporal lobe seizures are known to cause impairments in hippocampus-dependent memory and reduce the number of place field selective neurons in the CA1 and their place field stability (Liu et al. 2003). Although memory impairment due to spontaneous seizure events in our mice cannot be excluded, seizures were never observed in any DBA/2J mouse during behavioral assays or in the home cage (HC) during daily checks on animal welfare.

To assess potential mouse strain differences in the effect of a behaviorally relevant and less harmful stimulus we next analyzed in vivo IEG expression following SOR training. The hippocampal subregions CA1, CA3, and dentate gyrus (DG) were analyzed separately due to their involvement in different aspects of memory acquisition and consolidation (Daumas et al. 2005; McAvoy et al. 2015). We also investigated cortical regions known for their in-

volvement in the SOR task; namely, the retrosplenial cortex (RSC), parietal cortex (PC) and prefrontal cortex (PFC) (Barker et al. 2007; Kesner 2009; de Landeta et al. 2020). In addition to the IEGs, *Arc*, *Npas4*, and *Nr4a1* assessed in our primary cultures, we characterized the expression of a further three IEGs activated by nuclear calcium signaling and activation of the CREB/CBP transcription factor complex, *Bdnf*, *cFos*, and *Inhba* (Zhang et al. 2009). A single time point of 30 min after SOR training was used.

Despite multiple behavioral differences and deficits in hippocampal-dependent learning in DBA/2J mice, we did not find a global impairment in the basal expression of IEGs or their induction by SOR training but instead selective differences in basal or SOR induced expression of some IEGs in certain brain regions. Basal IEG expression in untrained home cage (HC) animals did not differ between C57BL/6N and DBA/2J strains in any hippocampal or cortical region for any gene except for *Inhba*, which showed a significantly elevated basal expression in the CA1 region of DBA/2N mice ($P = 0.0089$) and a trend for elevated expression in CA3 ($P = 0.1149$) and DG ($P = 0.0585$) (Table 2; Figs. 5, 6). SOR learning-evoked induction of *Arc*, *c-Fos*, and *Nr4a1* IEGs involved in memory formation (Fleischmann et al. 2003; Tzingounis and Nicoll 2006; McNulty et al. 2012) occurred in both C57BL/6N and DBA/2J mice in all analyzed hippocampal and cortical regions with no difference in their induction levels between strains when normalized to the HC mice of the same strain. SOR training also significantly induced *Bdnf* expression in both mouse strains in most brain regions, however, with low and variable levels most likely due to the relatively early 30-min time point of our sample relative to the delayed induction kinetics for this IEG (Sun and Lin 2016). *Npas4*, another well characterized IEG important for spatial and contextual learning (Ramamoorthi et al. 2011; Coutellier et al. 2012; Weng et al. 2018), was also significantly induced by SOR training in both mouse strains in the CA3, DG, RSC, and PC but DBA/2J mice showed higher SOR induction of *Npas4* in the CA3 than C57BL/6N mice ($P = 0.032$) and DBA/2J mice showed SOR induction of *Npas4* in the CA1 and PFC where induction in C57BL/6N mice was absent. The increased basal expression of *Inhba* in DBA/2J mice in all hippocampal regions reported above was accompanied by an absence of *Inhba* induction by SOR training selectively in the DG and PC in DBA/2J but not C57BL/6N mice. The PC of DBA/2J mice showed attenuated learning-induced expression for all analyzed genes when normalized to C57BL/6N
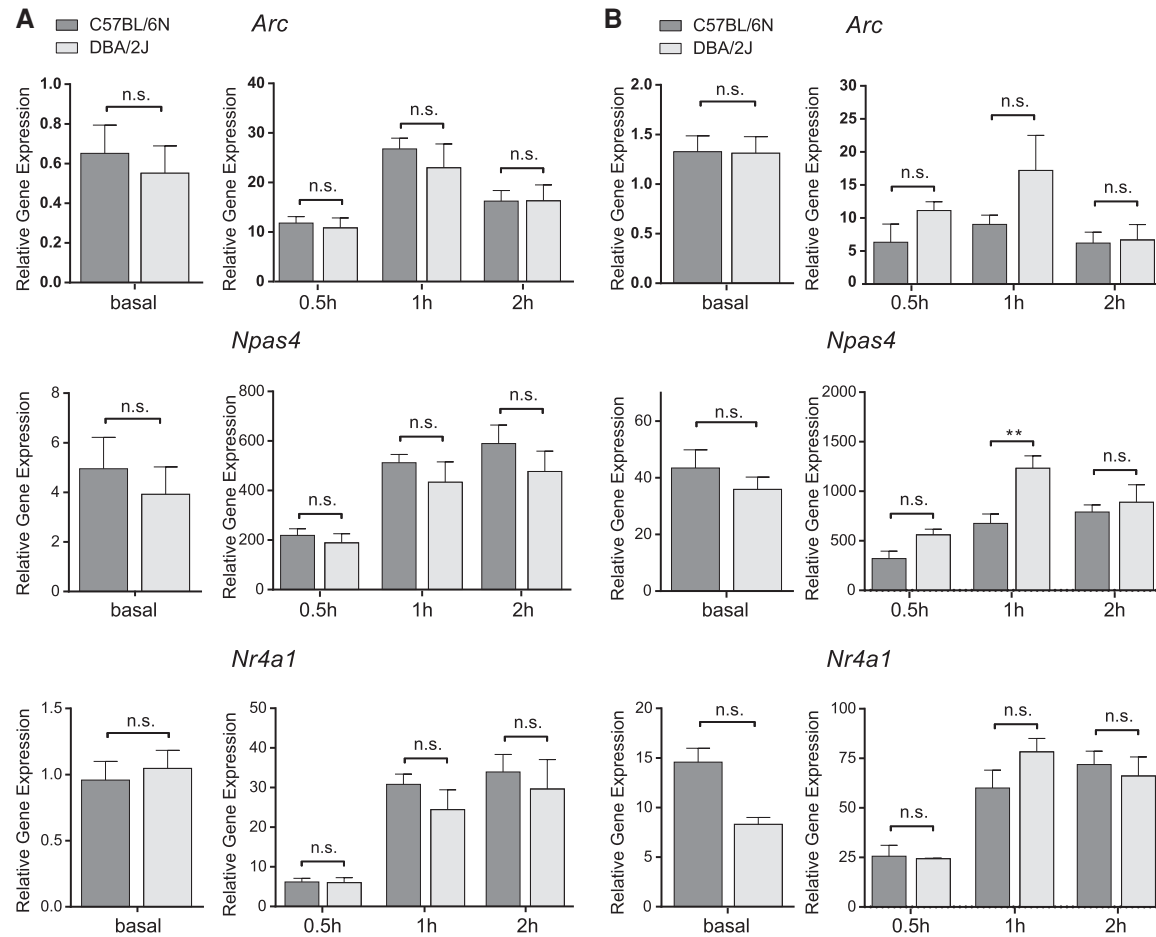
Figure 3. IEG induction in primary neuronal cultures. (*A,B*) RT-qPCR analysis of IEG expression in primary hippocampal (*A*) and cortical (*B*) cultures. Panels at the *left* show the basal gene expression of the respective gene. Panels at the *right* show relative gene expression of IEGs *Arc*, *Npas4*, and *Nr4a1* after 0.5-, 1-, and 2-h bicuculline (50 µM) treatment of primary neuronal cultures from C57BL/6N and DBA/2J P0 mice after 10–11 d in culture. *Gusb* was used as the endogenous control and expression was normalized to total brain RNA pooled from both mouse strains. DBA/2J $n = 6$ mice; C57BL/6N $n = 8$ mice. Graphs show mean ± SD Statistical significance was determined by one-way ANOVA with Tukey's multiple comparison test. (n.s.) Not significant, (**) $P < 0.01$.

HC controls with significant induction differences between strains for *Bdnf* and *Inhba*. In contrast, IEG expression and induction in the PFC and RSC did not differ between the strains for all analyzed genes.

In summary, in vivo IEG expression data shows that the spatial learning-impaired DBA/2J show elevated basal and reduced SOR training induced expression of *Inhba* in the hippocampus and PC, and elevated SOR induction of *Npas4* in the hippocampus. Since *Inhba* can prolong long-term potentiation in CA1 pyramidal neurons (Ageta et al. 2010; Hasegawa et al. 2014) and *Npas4* expression regulates both excitatory and inhibitory synaptic connectivity in the hippocampus (Lin et al. 2008; Sim et al. 2013; Spiegel et al. 2014), we next investigated synaptic function in the CA1.

DBA/2J show reduced inhibitory and increased excitatory basal synaptic input onto hippocampal CA1 pyramidal neurons

To analyze inhibitory and excitatory synaptic connectivity we recorded, in acute hippocampal slices (ex vivo) from untrained HC mice, miniature inhibitory postsynaptic currents (mIPSCs)
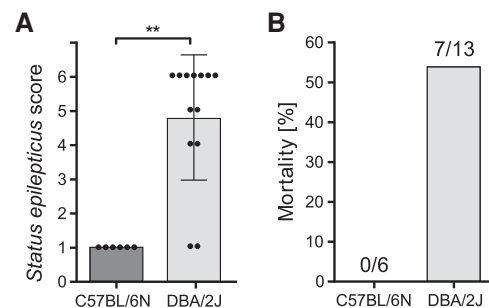

Figure 4. Kainic acid administration in vivo. (*A*) Status epilepticus score and (*B*) mortality rate of DBA/2J and C57BL/6N after kainic acid administration. The panel on the *left* shows the number of mice deceased after i.p. administration of 15 mg/kg body weight kainic acid. On the *right* the status epilepticus severity is shown, scored as follows: 0: no reaction; 1: immobility; 2: sudden shaking, chewing movements; 3: clonus of front extremities; 4: erecting of the body; 5: continuous body erection, seizures; and 6: death. DBA/2J $n = 13$; C57BL/6N $n = 6$. Graphs show percentage (*A*) and mean ± SD (*B*). (*B*) Statistical significance was determined by Mann–Whitney test. (*) $P < 0.05$, (**) $P < 0.01$, (***) $P < 0.001$.

Table 2. In vivo RT-qPCR statistical results summary comparing C57BL/6N and DBA/2J mice

			Arc	*Bdnf*	*c-Fos*	*Inhba*	*Npas4*	*Nr4a1*
CA1	Basal	B6 Vs D2	n.s.	n.s.	n.s.	**	n.s.	n.s.
	SOR	B6	***	**	***	n.s.	n.s.	**
		D2	***	***	***	n.s.	**	**
		B6 Vs D2	n.s.	n.s.	n.s.	*	*	n.s.
		B6 Vs D2#	n.s.	n.s.	n.s.	n.s.	n.s.	n.s.
CA3	Basal	B6 Vs D2	n.s.	n.s.	n.s.	p = 0.115	n.s.	n.s.
	SOR	B6	***	***	***	n.s.	***	***
		D2	***	n.s.	***	n.s.	***	***
		B6 Vs D2	n.s.	n.s.	n.s.	n.s.	n.s.	n.s.
		B6 Vs D2#	n.s.	n.s.	n.s.	n.s.	*	n.s.
DG	Basal	B6 Vs D2	n.s.	n.s.	n.s.	p = 0.058	n.s.	n.s.
	SOR	B6	***	***	***	***	***	***
		D2	***	**	***	n.s.	***	***
		B6 Vs D2	**	n.s.	*	n.s.	**	n.s.
		B6 Vs D2#	n.s.	n.s.	n.s.	*	n.s.	n.s.
RSC	Basal	B6 Vs D2	n.s.	n.s.	n.s.	n.s.	n.s.	n.s.
	SOR	B6	**	***	***	n.s.	***	***
		D2	***	**	***	n.s.	**	***
		B6 Vs D2	n.s.	n.s.	n.s.	n.s.	n.s.	n.s.
		B6 Vs D2#	n.s.	n.s.	n.s.	n.s.	n.s.	n.s.
PC	Basal	B6 Vs D2	n.s.	n.s.	n.s.	n.s.	n.s.	n.s.
	SOR	B6	***	***	***	*	***	***
		D2	***	***	***	n.s.	***	***
		B6 Vs D2	**	n.s.	*	*	*	*
		B6 Vs D2#	n.s.	***	n.s.	*	n.s.	n.s.
PFC	Basal	B6 Vs D2	-	n.s.	n.s.	-	n.s.	n.s.
	SOR	B6	-	n.s.	**	-	n.s.	*
		D2	-	*	***	-	**	**
		B6 Vs D2	-	n.s.	n.s.	-	n.s.	n.s.
		B6 Vs D2#	-	n.s.	n.s.	-	n.s.	n.s.

Statistical results summary for six brain regions (CA1, CA3, DG, RSC, PC, and PFC) and six IEGs (*Arc, Bdnf, c-Fos, Inhba, Npas4*, and *Nr4a1*) comparing basal IEG expression between C57BL/6N (B6) and DBA/2J (D2) untrained HC animals (Basal row) and SOR induction of IEG expression by comparing SOR trained animals with untrained HC animals of the same strain (SOR B6 and SOR D2 rows). Between strain differences in SOR gene induction is indicated for normalization of both strains to the C57BL/6N HC animals (SOR B6 vs. D2 row) or when induction is normalized to the HC animals of the same strain (SOR B6 vs. D2# row). Higher basal or SOR induction in DBA/2J mice is indicated in green (nonsignificant trends indicated in light green), and lower basal or induction in DBA/2J mice is indicated in red. (n.s.) Not significant, (*) $P < 0.05$, (**) $P < 0.01$, (***) $P < 0.001$, (—) no data.

mediated by GABA$_A$ receptors (Fig. 7A–D) and miniature excitatory postsynaptic currents (mEPSCs) mediated by α-amino-3-hydroxy-5-methyl-4-isoxazolepropionic acid (AMPA) receptors (Fig. 7E–H). We found a longer interevent interval (IEI; the inverse of frequency) of mIPSCs ($t_{(39)} = 3.495$, $P = 0.0012$) (Fig. 7C) and a slightly shorter IEI of mEPSCs ($t_{(59)} = 2.610$, $P = 0.0115$) (Fig. 7G) in CA1 neurons of DBA/2J mice. These differences were not accompanied by any change in mIPSC amplitude ($t_{(39)} = 1.889$, $P = 0.0664$) (Fig. 7D) or mEPSC amplitude ($t_{(59)} = 1.17$, $P = 0.2458$) (Fig. 7H). These differences in mIPSC and mEPSC frequency in the absence of differences in amplitude are likely to reflect a reduced number of inhibitory synapses or their release probability and an increased number of excitatory synapses or their release probability at pyramidal neurons in the CA1 region of the hippocampus of DBA/2J mice.

Discussion

This study brings together a broad assessment of the behavioral phenotype, the activity and learning induced IEG expression profile as well as morphological and electrophysiological characterization of the learning-deficient inbred mouse strain, DBA/2J. We show that the DBA/2J memory deficits include hippocampus-dependent CFC and SOR, an impairment in the striatum-dependent VMCL task and increased anxiety-like behavior. Thus, the learning impairment of DBA/2J is broader than previously thought and can be partly explained by a working memory or acquisition deficit as has previously been suggested (Beddeley and Hitch 1974; Schwegler et al. 1990). The impairment in both STM and LTM for CFC indicate impaired learning likely resulting from nonspecific anxiety and hyperactivity. The LTM-specific deficit of SOR reflects the insensitivity of this assay to anxiety and hyperactivity and makes it attractive for transcriptional profiling of the transcription-dependent memory impairments in the DBA/2J mouse strain independent of such confounds.

Dysfunction of the PC and DG in DBA/2J mice

The normal baseline IEG expression levels and the C57BL/6-like induction or superinduction of IEGs either by synaptic activity in primary cultures or by SOR training in vivo for most genes in most brain regions indicates the absence of any overriding deficit for cellular signaling pathways or spatial exploration in DBA/2J mice. Poor LTM for SOR in DBA/2J mice was associated with deficits in SOR-induced gene expression restricted to the PC while SOR induction of most IEGs was enhanced in the hippocampus DG. The impaired IEG induction by SOR in the PC suggests a reduced activation of this region by spatial novelty in DBA/2J mice, which may explain why lesions of this region do not further impair their performance in the SOR task (Thinus-Blanc et al. 1996). The superinduction following SOR training of multiple activity-dependent IEGs in the DG may result from impaired polysynaptic inhibition in the DBA/2J DG (Bampton et al. 1999), which would amplify responses to repetitive excitatory stimuli and is proposed to underlie the impaired maintenance of LTP in the DG of DBA/2J mice (Bampton et al. 1999; Jones et al. 2001). These strain-dependent alterations in DG and PC IEG activation suggest a critical role of these regions in spatial novelty-induced LTM and may partly underlie the observed SOR impairment in DBA/2J mice.

Role of *Npas4* and *Inhba* in learning and synaptic connectivity

From our in vivo IEG results, the superinduction of *Npas4* by SOR training and the increased basal *Inhba* expression were particularly compelling, since both alterations occurred in hippocampal but not cortical regions indicating a special relevance of those two genes for hippocampal function and spatial novelty learning. Intriguingly, both *Npas4* and *Inhba* regulate synaptic connectivity in the hippocampus. The neuron-specific IEG *Npas4* is regulated by neuronal activity and nuclear calcium signaling (Lin et al. 2008; Zhang et al. 2009; Spiegel et al. 2014; Sun and Lin 2016) and regulates glutamatergic and GABAergic synapse development
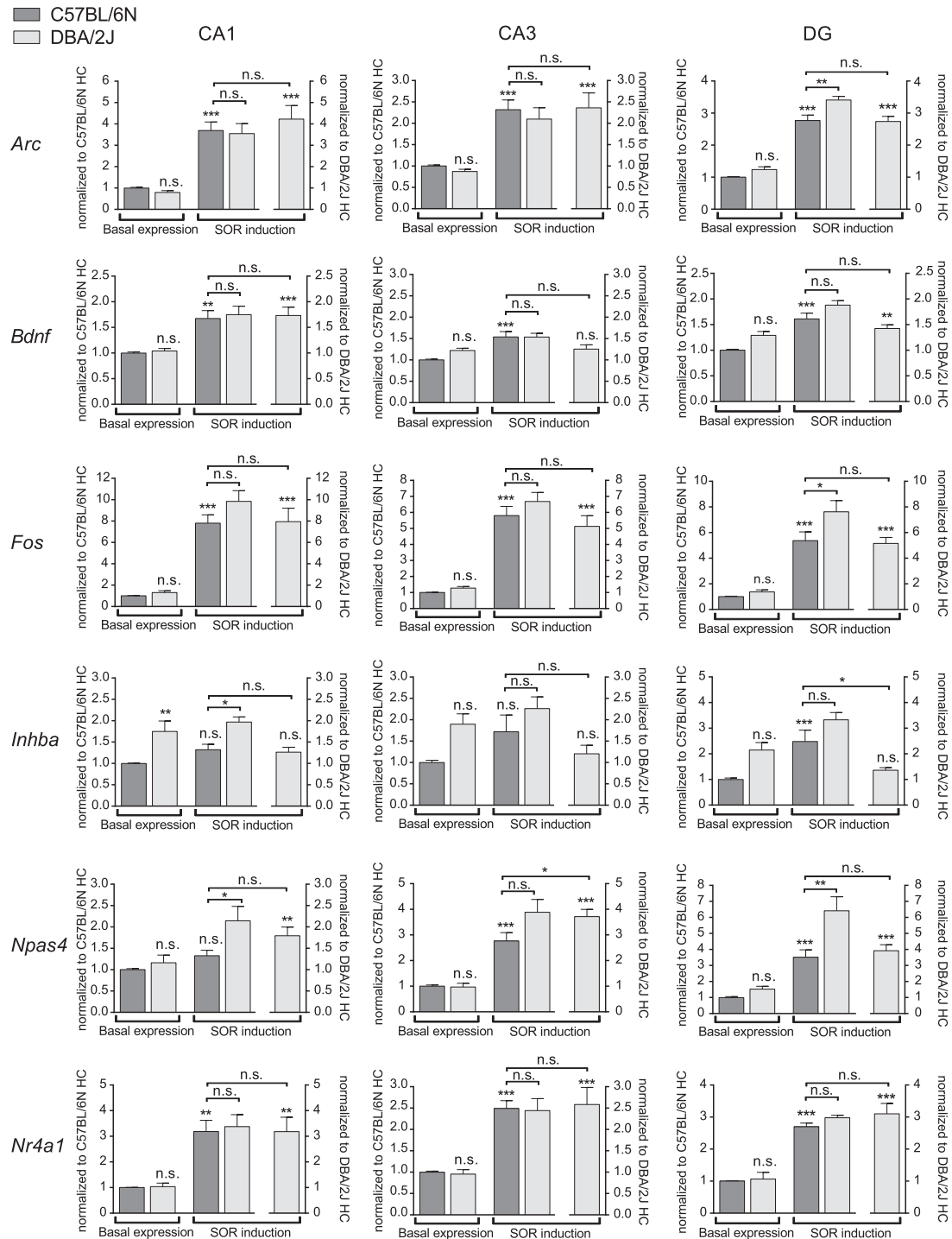
Figure 5. In vivo IEG induction in the hippocampus after SOR training. RT-qPCR analysis of IEG expression of *Arc, Bdnf, Fos, Inhba, Npas4,* and *Nr4a1* 30 min after completion of SOR training in hippocampal CA1, CA3, and DG regions. *Gusb* was used as endogenous control and expression was normalized to C57BL/6N home cage (HC) animals (*left* axis) or to DBA/2J HC animals (*right* axis). DBA/2J $n = 7$; C57BL/6N $n = 7$. Graphs are plotted as mean ± SEM. Statistical significance was determined by one-way ANOVA with Tukey's multiple comparison test. (n.s.) Not significant, (*) $P < 0.05$, (**) $P < 0.01$, (***) $P < 0.001$.

in both glutamatergic and GABAergic neurons (Lin et al. 2008; Sim et al. 2013; Spiegel et al. 2014). *Inhba* encodes Activin A, which is neurotrophic and known to promote dendritic complexity in glutamatergic hippocampal granule cells but reduce tonic GABAergic inhibition (Iwahori et al. 1997; Muller

et al. 2006; Sekiguchi et al. 2009; Krieglstein et al. 2011). *Inhba* is selectively induced by SOR training in the DG in C57B/6N animals but not in DBA/2J mice where *Inhba* is already up-regulated in untrained HC animals thereby occluding to some degree its further induction by SOR.
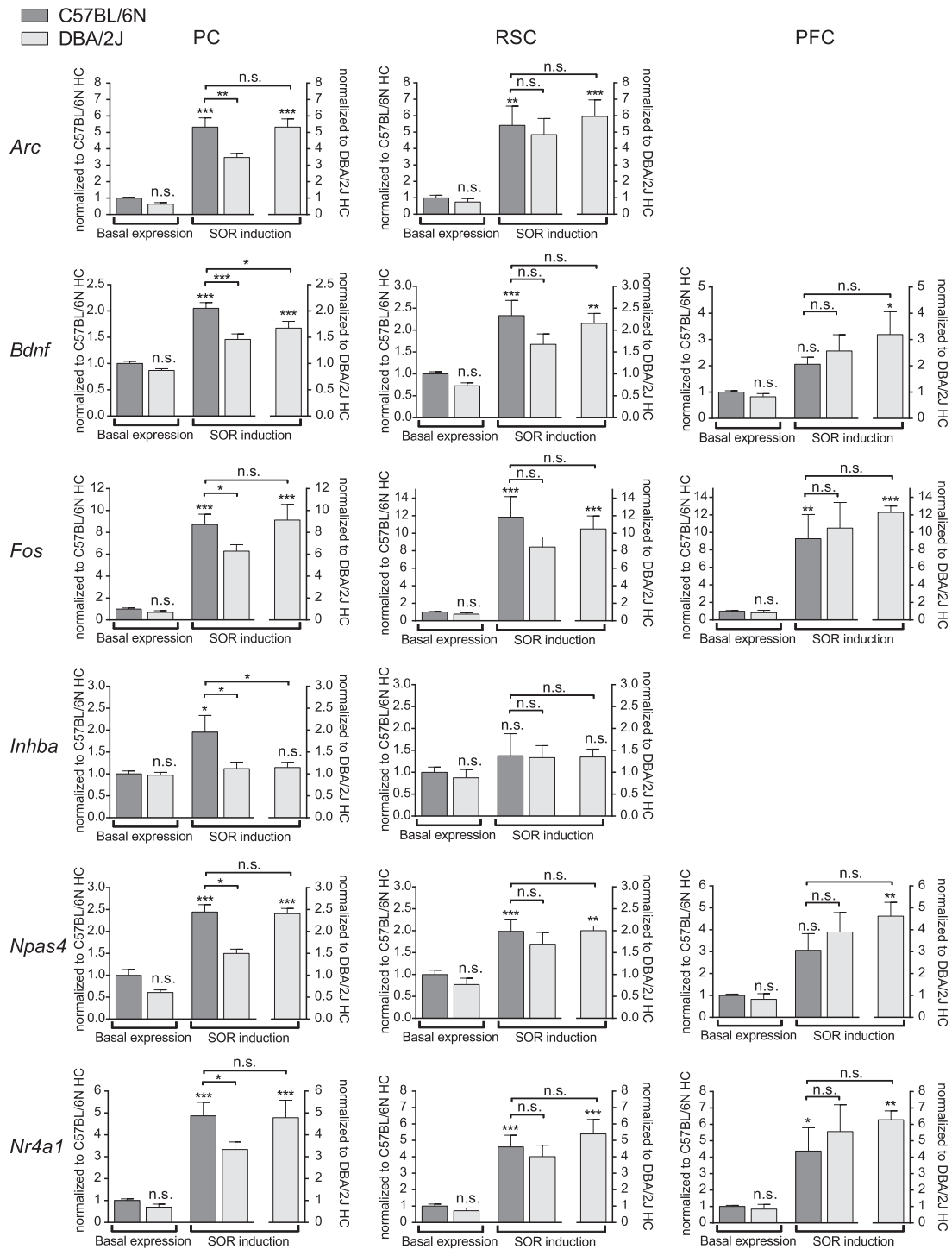
Figure 6. In vivo IEG induction in cortical regions after SOR training. RT-qPCR analysis of IEG expression of *Arc*, *Bdnf*, *Fos*, *Inhba*, *Npas4*, and *Nr4a1* 30 min after completion of SOR training in parietal cortex (PC), retrosplenial cortex (RSC), and prefrontal cortex (PFC). *Gusb* was used as endogenous control and expression was normalized to C57BL/6N home cage (HC) animals (*left* axes) or to DBA/2J HC animals (*right* axes). DBA/2J $n = 7$; C57BL/6N $n = 7$. Graphs are plotted as mean ± SEM. Statistical significance was determined by one-way ANOVA with Tukey's multiple comparison test. (n.s.) Not significant, (*) $P < 0.05$, (**) $P < 0.01$, (***) $P < 0.001$.

We found reduced inhibitory and enhanced excitatory synaptic input to CA1 pyramidal neurons of untrained DBA/2J mice indicating a positive shift in the excitation–inhibition balance arising from neurotransmitter selective differences in synaptic con-

nectivity or release probability (see below). Thus, the elevated *Inhba* expression throughout the hippocampus in untrained HC DBA/2J mice may underlie this observed excitation–inhibition shift. Although *Npas4* expression regulates the excitation–
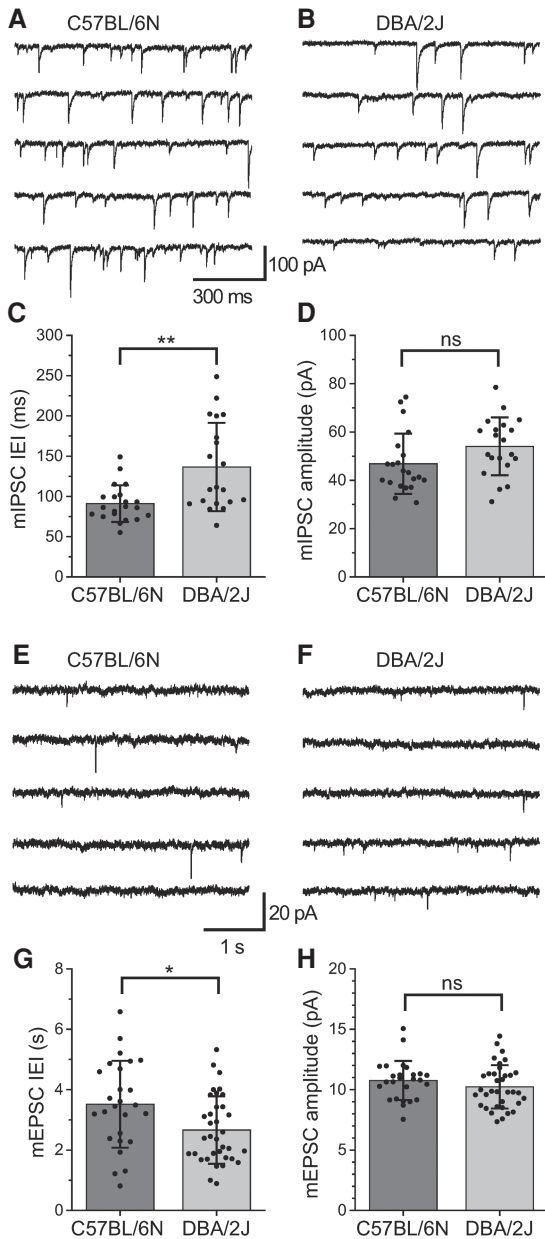
Figure 7. mIPSC and mEPSC data of CA1 pyramidal neurons from DBA/2J and C57BL/6N mice. Representative whole-cell patch clamp recordings (Vhold = −70 mV) and summary statistics for the amplitude and interevent interval (IEI) of miniature inhibitory postsynaptic currents (mIPSC) (*A–D*) and miniature excitatory postsynaptic currents (mEPSC) (*E–H*) of CA1 pyramidal neurons from C57BL/6N and DBA/2J mice. Histograms show mean values for individual cells and their mean ± SEM. Statistical significance was determined by independent, two-tailed *t*-test. (ns) Not significant, (*) $P < 0.05$, (**) $P < 0.01$. See Table 1.

inhibition balance in synaptic connectivity, no significant strain-dependent differences in the basal expression of *Npas4* in un-trained HC animals were observed. *Npas4*, however, did show superinduction by SOR in the hippocampus of DBA/J2 mice. It is tempting to speculate that this results from the excitatory shift in synaptic connectivity in the basal, untrained state that would prime the network for activity-induced nuclear calcium signals and *Npas4* transcription following SOR training. However, other nuclear calcium activity-regulated IEGs in the same hippocampal

regions were not superinduced by SOR. This might indicate that *Npas4* is more sensitive toward changes in the excitation–inhibition balance than other IEGs. The single time point used in this study (30 min after SOR training) may have been too early to detect the peak transcriptional response of effector genes such as *Bdnf*, the expression of which is known to be strongly enhanced by the immediate early response transcription factor *Npas4* (Pruunsild et al. 2011).

Altered excitation–inhibition balance may underlie seizure susceptibility and learning impairments

The differences in mEPSC and mIPSC frequency but not amplitude we observed in the CA1 are likely to reflect differences in the number of functional synapses or the vesicle release probability for glutamatergic and GABAergic synapses, respectively. A reduced instantaneous release probability of glutamatergic synapses has been reported for the CA1 of DBA/2J mice (Lenselink et al. 2015) but no difference was found in the DG (Bampton et al. 1999). It is possible that such strain-dependent differences are region-specific since no differences in mIPSC or sIPSC frequency occur in cortical layer 2/3 pyramidal neurons and increased mIPSC frequency has been reported in the thalamus of DBA/2 mice (Tan et al. 2007, 2008). It remains unclear whether the synaptic differences observed here in the CA1 of DBA/2J mice underlie impairments in the induction or maintenance of synaptic plasticity. A DBA/2 deficit in LTP maintenance (late phase > 1 h) has been shown for theta burst and some tetanic stimulation protocols for the Schaffer collateral inputs to CA1 pyramidal cells (Matsuyama et al. 1997; Nguyen et al. 2000a,b; Jones et al. 2001; Gerlai 2002; Schimanski and Nguyen 2005). While an increase in glutamatergic and a decrease in GABAergic synaptic inputs to CA1 pyramidal neurons would predict an enhanced potential for LTP, disruptions elsewhere in the vesicle reserve pool, feedforward and feedback network connectivity or the induction of IEGs reported here may be responsible for the impaired LTP maintenance in DBA/2J mice.

Reduced GABAergic synaptic function has further consequences for hippocampal function, including reduced feedforward inhibition critical for counterbalancing bursts of excitatory activity causing seizures (Bernard 2012). Elevated expression of some neuronal activity-dependent IEGs during learning together with an increased seizure susceptibility after kainic acid administration and other stimuli such as sound (Le Gal La Salle and Naquet 1990; McLin and Steward 2006) may result from the elevated excitation–inhibition balance in the hippocampal network of DBA/2J mice. Feedforward inhibition is also required for brain oscillations associated with memory consolidation (Roux and Buzsaki 2015). The excitation–inhibition ratio for synaptic input in the hippocampus is critical for sharp-wave ripple activity and learning and memory (Valero et al. 2017; Lucas and Clem 2018). In recent years the significance of impaired excitation–inhibition balance became the focus of research in a broad range of neurodevelopmental and also neurodegenerative disorders with diverse molecular mechanisms being proposed (Foss-Feig et al. 2017; Del Pino et al. 2018). Its relevance for age-dependent memory decline in humans is also becoming increasingly apparent (Lee et al. 2015; Robitsek et al. 2015; Barron et al. 2016; Legon et al. 2016). Thus, disturbances in feedforward inhibition and the excitation–inhibition balance in the hippocampus may be involved in the behavioral deficits of the DBA/2J strain.

The larger AHP amplitude of DBA/2J CA1 pyramidal neurons suggests the stronger activation of the BK and SK calcium-activated potassium channels primarily responsible for the AHP in this neuron type. Such increased channel activation may arise from a stronger AP-induced calcium influx, a higher calcium channel density

or reduced calcium buffering. Although differences in accommodation or depolarization induced AP generation were not detected in DBA/2J mice, a dampening effect on higher frequency burst firing, such as responses to strong synaptic input, could potentially affect learning induced AP generation in the CA1. Indeed, a larger postburst AHP amplitude in CA1 pyramidal neurons is associated with age-related cognitive decline in rats (Oh et al. 2016). The roles of such mechanisms in DBA/2J learning deficits require further investigation.

The selective breeding used to create the first inbred mouse strain generated a distinct genetic background of the DBA/2 line that bestowed it with several behavioral anomalies. This study further defines hippocampus-dependent and hippocampus-independent learning deficits in this mouse strain and reveals IEG-specific and brain region-specific differences in transcriptional responses to the SOR learning task that cannot be attributed to confounding differences in anxiety and hyperactivity. We show a probable link between a selective LTM deficit for the hippocampus-dependent SOR learning paradigm in DBA/2J and the transcriptional dysregulation of *Npas4* and *Inhba* in the hippocampus paired with a positive shift in the excitation–inhibition balance of synaptic connections in the CA1. These results highlight the specific molecular and cellular underpinnings of deficits in learning and memory resulting from genetic variability.

Materials and Methods

Compliance with ARRIVE guidelines

Experimental design and reporting standards comply with the guidelines for Animal Research: Reporting In Vivo Experiments (ARRIVE) (Kilkenny et al. 2010). Biostatistical and biometrical planning was guided by the Department of Medical Biometry at the Institute of Medical Biometry and Informatics at Heidelberg University. Power calculations of animal numbers were done prior to starting the study. Sample sizes were calculated using SAS version 9.1 proc power to ensure adequate power with an effect size of 0.8.

Mice

We used 3-mo-old (young adult) male DBA/2J (Janviere) and C57BL/6N (Charles River) mice for all in vivo and ex vivo experiments. Mice were group-housed (four animals/group) on a 12-h light–dark cycle and had ad libidum access to water and food. Each cage (15 × 21 × 13.5 cm) contained one square cotton-nestlet as nesting material. Before behavioral testing, mice were housed 1 wk in our housing room (Neurobiology, Heidelberg University). A total of 211 mice were used for this study, 172 underwent behavioral paradigms, and 39 were used for structural and electrophysiological analyses. Health status was checked daily. Sick or injured mice were excluded from the study. Spatial memory and anxiety experiments were performed during the light phase (8 a.m. to 6 p.m.). Mice used for VMCL experiments were single-housed under a reversed dark/light cycle and tested during the dark cycle. During operant conditioning, food supply was restricted to maintain 85%–90% of the free-feeding body weight of each mouse as previously described (Richter et al. 2014; Mallien et al. 2016; Koppe et al. 2017).

Contextual fear conditioning

For 3 d prior to training, mice were habituated to the experiment room 0.5 h per day and handled 2 min per day. On the training day, mice were placed into the conditioning chamber (23 × 23 × 35 cm, TSE) and 148 sec later received a 2-sec foot shock (0.7 mA) before being returned to their home cage 30 sec later. One hour (STM) or 24 h (LTM) after conditioning mice were tested with one 5-min exposure to the same context in the absence of foot shock. Freezing, defined as absence of movement except for respiration, was scored manually and continuously during training

and testing sessions. Mean velocity was scored automatically by TSE fear conditioning system software during training sand test sessions.

Spatial object recognition

For 3 d prior to training, mice were habituated to the experiment room 0.5 h per day and handled 2 min per day. The experimental arena consisted of a black, square box (50 cm × 50 cm × 50 cm) with a visual cue placed on one wall. Mice received one habituation session without objects and three training sessions with two objects (a glass bottle and a metal tower) in the arena. Each session lasted 6 min and between sessions, mice were returned to their home cage for 3 min, during which the arena was cleaned with 70% ethanol. One hour (STM) or 24 h (LTM) after training mice were tested by returning them to the arena with one of the objects in a new spatial location. Time spent exploring each object was manually scored during both the training and testing phases. Preference for the displaced object was calculated as a percentage of the total time exploring either objects during the test session as follows: exploration time of relocated object = $t_{displaced}$ [s]/($t_{nondisplaced}$ [s] + $t_{displaced}$ [s]) × 100 [%], where $t_{displaced}$ and $t_{nondisplaced}$ represent the time spent exploring the displaced and nondisplaced objects, respectively.

Gene expression analysis after spatial object recognition

For in vivo analysis, half of the animals per cage were randomly assigned to the control group (home cage animals) and were handled and placed in the behavior room on the training day, but they were not subjected to training and remained in their cage. Brains were collected 30 min after behavioral training and control brains were collected within 1 h of euthanizing the trained animals to minimize possible differences due to circadian rhythm. Mice were sacrificed by cervical dislocation, and brains were rapidly removed and cut in coronal sections (1 mm thick) using a brain matrix. Brain sections were stored in RNAlater (Sigma Life Science) for 1 wk before microdissecting individual brain regions using a binocular microscope (Stemi SV6, Zeiss). Tissue was stored at –80°C until total RNA extraction.

Open field

The open field test was quantified from the 6-min habituation session before spatial acquisition training (see above) using Smart Video tracking software (Panlab, Harvard Apparatus). Anxiety-like behavior of the mice was quantified as total number of entries into the central zone (*n*, the central 32% of the arena), the percentage of the time spent in the central zone (100% × t_{center}/t_{total}), the latency to the first entry into the central zone and the distance traveled in the central zone (100% × distance$_{central}$/distance$_{total}$).

Nesting

Nest building ability was quantified as a nesting score described by Deacon (2006) 1 wk after contextual fear conditioning. In short, mice were placed overnight with one cotton square nestlet (Plexx B.V.) in separate cages. After 12 h, nest quality was scored according to the Deacon scoring system and the untorn nesting material was weighted. The mass of the untorn nestlet was calculated as follows: (weight of nestlet after separation/weight of nestlet before separation) × 100%.

Visuomotor conditional learning

Apparatus

The VMCL and Pokey training were assessed in Bussey–Saskida operant touchscreen chambers (Campden Instruments Ltd. 80614-20). The trapezoid chambers (19 cm high, 24 wide, respectively, 6 cm, 17 cm deep) consisted of black Perspex walls and a metal grid floor and were equipped with a liquid dispenser tray with illumination on the short end and a screen on the opposing

wall. The liquid dispenser delivered the palatable reward solution (sweetened condensed milk [Milchmädchen, Nestle] diluted 1:4 with tap water). A black Perspex mask separated the screen into three touch-sensitive fields (7 × 7 cm), which could display visual cues and detect touch responses. A light was mounted above the chamber and a tone generator was installed in the chamber. Software (ABET II Touch software) controlled the functions of chamber components and detected the behavioral responses.

Pokey training

The Pokey training procedure was performed as previously described (Talpos et al. 2009; Horner et al. 2013; Richter et al. 2014). After an habituation session (20 min with access to sweetened condensed milk), the mice were familiarized with the functions of the box in successive training phases: (1) the presentation of a stimulus (a white square) on one of three fields (center, left, and right) of the touch screen, (2) the association of reward delivery with a tone, (3) the touch of the touch field displaying the stimulus to trigger reward delivery, (4) the entry into the food tray as a prerequisite to initiate the next trial, (5) the punishment of an incorrect response (touching a touch field without stimulus presentation) by a 5-sec time-out with illumination of the chamber, and (6) the touch of the center field to initiate a choice phase where instead of reward delivery, stimuli appeared on either the left or the right field and touching these resulted in reward presentation.

VMCL

The VMCL protocol was adapted from Delotterie et al. (2015). Briefly, the task is to identify visual stimuli presented in the center of the screen that indicate whether to touch the left or the right of the screen in order to receive a reward, following the rule "If stimulus A, then go left; if stimulus B, then go right." In the choice phase one of two distinct visual stimuli (white icicle or white equal sign) appeared in a pseudorandom order and the direction indicated by each visual stimulus was reversed for half the animals in each experimental group. A touch of the correct side of the screen triggered the delivery of a reward, tray illumination and tone generation, whereas a touch to the incorrect side of the screen triggered the 5-sec time-out with illumination of the arena. Incorrect responses caused a correction trial, in which the previous trial was repeated until the correct response was given. Correction trials were not counted into the measure of accuracy. After a 5-sec intertrial interval, the mouse could initiate the next trial. Subjects were tested for 15 d with one session per day and 30 trials per session with a maximum duration of 60 min. We counterbalanced the direction of the reward indicating visual stimuli between the groups: Half the mice learned to touch the left field when presented with the white icicle and touch the right field when the white equal appeared, while the other half learned the opposite rule.

Visible platform water maze

A visual version of the water maze was used as described previously (Belz et al. 2007) with modifications. The setup consisted of a water-filled (24°C) circular pool (150 cm in diameter), a black platform (14 × 14 cm²) and an orange and black colored 15-mL centrifuge tube, which was placed on the platform and served as a visual cue to indicate the position of the platform from afar. Mice habituated to the experimental room 0.5 h before the experiment started. We assessed the latency to reach the platform for each mouse in four trials. The platform position changed between the trials to circumvent orientation with other cues. We adapted the start position in each trial, keeping the distance from entry point to platform identical. The direction of the quickest path was counterbalanced, thereby having the shortest distance twice to the left and twice to the right side in a random order. Each trial ended when the mouse reached the platform or after 2 min. Mice were placed in front of a warming light for 5 min and then returned to their home cage for an additional 40 min between trials.

Kainic acid administration

Mice were injected with kainic acid (15 mg/kg body weight i.p.; Sigma-Aldrich) in PBS (injection volume 4 mL/kg body weight). Control mice from each strain received i.p. injections of PBS only. Injected mice were put in a black bin (25 cm × 30 cm × 60 cm) to avoid self-injury due to seizures. Mice were observed during the following 30 min and severity of seizures was scored according to the following status epilepticus scoring system: 0: no reaction; 1: immobility; 2: sudden shaking, chewing movements; 3: clonus of front extremities; 4: erecting of the body; 5: continuous body erection, seizures; and 6: death. After 30 min, mice were sacrificed via cervical dislocation and the brain was removed and stored for gene expression analysis.

Cell culture

Hippocampal and cortical neurons from newborn DBA/2J (Janvier) and C57Bl/6N (Charles River) mice were prepared, plated ($0.7 × 10^6$ cells/mL) and maintained as previously described (Bading and Greenberg 1991), except that growth medium was supplemented with B27 (Invitrogen/BRL) and 1% (v/v) rat serum. Experiments were performed at 10 and 11 d in vitro. For GABA$_A$ receptor inhibition and activation of synaptic activity from recurrent bursts of APs 50 μM bicuculline (Alexis Biochemicals) was used.

RT-qPCR

Total RNA was isolated using RNeasy Plus minikit (Qiagen) with additional on-column DNase I digestion according to the manufacturer's instructions. For the generation of cDNA, 1 μg of total RNA was reverse transcribed with the high-capacity cDNA reverse transcription kit (Invitrogen). Quantitative RT-PCR was performed on a StepOnePlus (Applied Biosystems) thermal cycler using TaqMan gene expression assays (Applied Biosystems) for the following genes: *Arc* (Mm00479619_g1), *Bdnf* (Mm00432069_m1), *c-Fos* (Mm00487425_m1), *Inhba* (Mm00434338_m1), *Npas4* (Mm00463644_m1), and *Nr4a1* (Mm00439358_m1). Expression levels of target genes were normalized to the expression of the housekeeping gene *Gusb* (Mm00446953_m1).

In vitro relative gene expression was normalized to mixed total brain RNA pooled from two C57BL/6N and two DBA/2J adults. In vivo relative gene expression data normalized to C57BL/6N was first normalized to one C57BL/6N HC animal from each training day and then normalized to the average of all C57BL/6N HC animals from the same day. In vivo relative gene expression data normalized to the respective HC animals for each mouse strain was performed the same way for C57BL/6N mice, and for DBA/2J mice data was normalized to a single DBA/2J HC animal from each training day and then normalized to the average of all DBA/2J HC animals from the same day.

Morphological analysis

Nissl staining

Brains were imbedded in tissue freezing medium (Leica Biosystems), cut into 20 μm thick slices with a Leica CM1950 cryostat at −18°C and stained according to Mulisch and Welsch (2010). Briefly, embedding medium was removed from slices by decreasing ethanol concentrations (100%, 90%, 70%, and 50%) and slices were treated with 50% (m/v) $K_2S_2O_5$ (in H_2O) for 5 min followed by a 10-min incubation in cresyl violet solution (1.5% [m/v] cresyl violet, 1% 1 M $C_2H_3NaO_2$, 1% 1 M acetic acid). Slices were then treated for 30 min in acetate buffer (0.1 M $C_2H_3NaO_2$, 0.1 M acetic acid at pH 4.6) before embedding in Xylol. All procedures except slicing were carried out at room temperature. Pictures were taken with an upright widefield Ni-E microscope with a 10× objective.

Golgi staining

For assessing dendritic morphology, 100 μm thick brain slices were stained with Golgi-Cox using the FD Rapid GolgiStain kit (FD NeuroTechnologies, Inc.) according to their protocol. Images

were acquired with a Nikon Ni-E microscope with a 20× objective. Total dendritic length of CA1 pyramidal neurons was calculated using Fiji (version 2.0.0) with macros written by E. Ruthazer (McGill University). Briefly, a *z*-stack acquisition was imported, calibrated and manually traced. For each strain, a minimum of four neurons per mouse from four mice was analyzed.

Electrophysiology

Acute slice preparation

Mice were anaesthetized with an intraperitoneal injection of pentobarbital (Narcoren, Merial) and perfused transcardially with slicing buffer [93 mM N-methyl-D-glucamine (NMDG), 93 mM HCl, 2.5 mM KCl, 1.2 mM NaH_2PO_4, 5 mM L(+)ascorbic acid, 2 mM thiourea, 3 mM sodium pyruvate, 10 mM $MgCl_2$, 0.5 mM $CaCl_2$, 20 mM HEPES, 30 mM $NaHCO_3$, 25 mM glucose, 10 mM N-acetyl-l-cysteine; gassed with 96% O_2 and 4% CO_2]. After decapitation, the brain was rapidly removed and submerged in ice-cold slicing buffer and 300-μm-thick coronal slices from the dorsal hippocampus were cut at 0°C (CU65 cooling unit; Microm HM650V Vibratome) and transferred to a 32°C holding chamber with slicing buffer. After 10 min, slices were transferred to room temperature artificial cerebrospinal fluid (aCSF; 125 mM NaCl, 3.5 mM KCl, 2.4 mM $CaCl_2$, 1.3 mM $MgCl_2$, 1.2 mM NaH_2PO_4, 25 mM glucose, 26 mM $NaHCO_3$; gassed with 96% O_2 and 4% CO_2) until used for recordings over the subsequent 4 h.

Electrophysiology recordings

Whole-cell patch clamp recordings were made from CA1 pyramidal cells in acute hippocampal slices secured with a platinum harp in the recording chamber (Science Products OAC-1) and submerged in continuously flowing (3 mL/min) aCSF maintained at 32°C–34°C with an in-line perfusion heater (Warner Instruments TC324B). Patch electrodes (3–5 MΩ) were made from 1.5-mm borosilicate glass and filled with a potassium-based internal solution (127 mM $KMeSO_4$, 0.2 mM EGTA, 10 mM HEPES, 10 mM K_2Phosphocreatine, 12 mM KCl, 8 mM NaCl, 4 mM Mg-ATP, 0.5 mM Na_3-GTP) except for miniature IPSC recordings, which used a cesium-based internal solution with symmetric chloride concentrations (130 mM CsCl, 10 mM HEPES, 5 mM EGTA, 20 mM CsOH, 0.5 mM $CaCl_2$, 4 mM Mg-ATP, 0.5 mM Na_3-GTP). MIPSCs were recorded at −70 mV in the presence of 10 μM AMPA receptor inhibitor 2,3-dioxo-6-nitro-1,2,3,4-tetrahydrobenzo[f]quinoxaline-7-sulfonamide disodium salt (NBQX; Biotrend) and 0.5 μM tetrodotoxin (TTX; Biotrend). The complete blockade of mIPSCs by 5 μM $GABA_A$ receptor antagonist gabazine-hydrobromide (Biotrend SR95531) was confirmed in five cells. MEPSCs were recorded in the presence of 0.5 μM TTX and their complete blockade by 10 μM NBQX was confirmed in three cells. Neurons recorded with the potassium based internal solution were identified as pyramidal by their slow firing rate and large, rounded AHP. Recordings were made with a Multiclamp 700A amplifier, digitized through a Digidata 1322A A/D converter and acquired and analyzed using pClamp 10 software (Molecular Devices). Voltage-clamp recordings were made at 5× gain, with a low-pass filter of 1 kHz and a sampling rate of 20 kHz. Current-clamp recordings were made at 10× gain with a lowpass filter of 10 and 20 kHz sampling rate. Pipette access resistance was maintained below 25 MΩ, range: 5–25 MΩ.

Electrophysiology analysis

Passive properties were monitored throughout the recordings and stabilized values were used for analysis. Spike threshold, AP amplitude, half width, afterhyperpolarization potential amplitude, and delay were calculated using the first AP elicited by a cell that fell within the duration of the depolarizing current injection from the resting membrane potential (i.e., not spontaneously elicited APs or any AP coinciding with stimulation onset). AP threshold was taken as the point where the first derivative of the voltage trace exceeded 20 mV/msec. AP amplitude and AHP were calculated relative to this threshold. Accommodation index was calculated as

the ratio of the time interval between the first and last pairs of APs in response to a 1-sec current injection evoking at least six APs. In eight cases (B6: three cells, D2: five cells), only four or five spikes could be elicited before showing total accommodation, and thus these were the traces used to calculate accommodation index. Rheobase current was the smallest current injection evoking an AP from resting membrane potential. HCN channels and Kir channels were activated with 1-sec hyperpolarizing steps from −50 to −120 mV in 10 mV increments. Kir conductance was quantified as the difference between slopes estimated by linear fits of the instantaneous current directly following the hyperpolarization-induced capacitive transient at −60 to −80 mV and −100 to −120 mV. HCN conductance was quantified as the slope of a linear fit of the difference between the instantaneous and steady-state currents at the end of the 1-sec hyperpolarization to −70 to −120 mV. MIPSC and mEPSC data were obtained from recordings of at least 200 events detected using the Mini Analysis Program (Synaptosoft). All events were visually verified and events occurring less than 10 msec after the previous event exhibited summation and were excluded from the amplitude but not the frequency analysis.

Statistical analysis

All graphs and statistical analyses were made with PrismTM 6.0 (GraphPad Software) or OriginPro 2016 (OriginLab). Figures were assembled in Adobe Illustrator 2015 (Adobe Systems, Inc.). Hypothesis tests and significance levels are indicated in the results text and figure legends. Normally distributed data was tested with two-tailed parametric Student's *t*-test in case of comparing two groups and one-way ANOVA with Tukey's multiple comparison in case of multiple group comparison. For in vitro expression shut-off experiments one-way ANOVA with repeated measures was used, since all samples stem from one culture preparation and were only treated differently. For every analysis, alpha was set to 0.05; therefore, $P > 0.05$ (n.s. [not significant]), $P < 0.05$ (*), $P < 0.01$ (**), and $P < 0.001$ (***).

Competing interests statement

The data sets used and/or analyzed during the current study are available from the corresponding author on reasonable request. The authors declare that they have no competing interests.

Acknowledgments

References

Abusaad I, MacKay D, Zhao J, Stanford P, Collier DA, Everall IP. 1999. Stereological estimation of the total number of neurons in the murine hippocampus using the optical disector. *J Comp Neurol* **408**: 560–566.

doi:10.1002/(SICI)1096-9861(19990614)408:4<560::AID-CNE9>3.0 .CO;2-P

Ageta H, Ikegami S, Miura M, Masuda M, Migishima R, Hino T, Takashima N, Murayama A, Sugino H, Setou M, et al. 2010. Activin plays a key role in the maintenance of long-term memory and late-LTP. *Learn Mem* **17:** 176–185. doi:10.1101/lm.16659010

Arnold FJ, Hofmann F, Bengtson CP, Wittmann M, Vanhoutte P, Bading H. 2005. Microelectrode array recordings of cultured hippocampal networks reveal a simple model for transcription and protein synthesis-dependent plasticity. *J Physiol* **564:** 3–19. doi:10.1113/jphysiol.2004.077446

Bading H. 2013. Nuclear calcium signalling in the regulation of brain function. *Nat Rev Neurosci* **14:** 593–608. doi:10.1038/nrn3531

Bading H, Greenberg ME. 1991. Stimulation of protein tyrosine phosphorylation by NMDA receptor activation. *Science* **253:** 912–914. doi:10.1126/science.1715095

Bading H, Ginty DD, Greenberg ME. 1993. Regulation of gene expression in hippocampal neurons by distinct calcium signaling pathways. *Science* **260:** 181–186. doi:10.1126/science.8097060

Bampton ET, Gray RA, Large CH. 1999. Electrophysiological characterisation of the dentate gyrus in five inbred strains of mouse. *Brain Res* **841:** 123–134. doi:10.1016/S0006-8993(99)01811-9

Barker GR, Bird F, Alexander V, Warburton EC. 2007. Recognition memory for objects, place, and temporal order: a disconnection analysis of the role of the medial prefrontal cortex and perirhinal cortex. *J Neurosci* **27:** 2948–2957. doi:10.1523/JNEUROSCI.5289-06.2007

Barrett RM, Malvaez M, Kramar E, Matheos DP, Arrizon A, Cabrera SM, Lynch G, Greene RW, Wood MA. 2011. Hippocampal focal knockout of CBP affects specific histone modifications, long-term potentiation, and long-term memory. *Neuropsychopharmacology* **36:** 1545–1556. doi:10.1038/npp.2011.61

Barron HC, Vogels TP, Emir UE, Makin TR, O'Shea J, Clare S, Jbabdi S, Dolan RJ, Behrens TE. 2016. Unmasking latent inhibitory connections in human cortex to reveal dormant cortical memories. *Neuron* **90:** 191–203. doi:10.1016/j.neuron.2016.02.031

Beddeley AD, Hitch G. 1974. Working memory. *Psychol Learn Motiv* **8:** 47–89. doi:10.1016/S0079-7421(08)60452-1

Belz S, Liu HK, Bock D, Takacs A, Vogt M, Wintermantel T, Brandwein C, Gass P, Greiner E, Schutz G. 2007. Inactivation of the gene for the nuclear receptor tailless in the brain preserving its function in the eye. *Eur J Neurosci* **26:** 2222–2227. doi:10.1111/j.1460-9568.2007.05841.x

Bernard C. 2012. Alterations in synaptic function in epilepsy. In *Jasper's Basic Mechanisms of the Epilepsies* (ed. Noebels JL, et al.), pp. 697–716. National Center for Biotechnology Information, Bethesda, MD.

Bridi MS, Abel T. 2013. The NR4A orphan nuclear receptors mediate transcription-dependent hippocampal synaptic plasticity. *Neurobiol Learn Mem* **105:** 151–158. doi:10.1016/j.nlm.2013.06.020

Brooks SP, Pask T, Jones L, Dunnett SB. 2005. Behavioural profiles of inbred mouse strains used as transgenic backgrounds. II: cognitive tests. *Genes Brain Behav* **4:** 307–317. doi:10.1111/j.1601-183X.2004.00109.x

Cabib S, Puglisi-Allegra S, Ventura R. 2002. The contribution of comparative studies in inbred strains of mice to the understanding of the hyperactive phenotype. *Behav Brain Res* **130:** 103–109. doi:10.1016/S0166-4328(01)00422-3

Cho WH, Park JC, Jeon WK, Cho J, Han JS. 2019. Superior place learning of C57BL/6 vs. DBA/2 mice following prior cued learning in the water maze depends on prefrontal cortical subregions. *Front Behav Neurosci* **13:** 11. doi:10.3389/fnbeh.2019.00011

Coutellier L, Beraki S, Ardestani PM, Saw NL, Shamloo M. 2012. Npas4: a neuronal transcription factor with a key role in social and cognitive functions relevant to developmental disorders. *PLoS ONE* **7:** e46604. doi:10.1371/journal.pone.0046604

Crusio WE, Schwegler H. 1987. Hippocampal mossy fiber distribution covaries with open-field habituation in the mouse. *Behav Brain Res* **26:** 153–158. doi:10.1016/0166-4328(87)90163-X

Daumas S, Halley H, Frances B, Lassalle JM. 2005. Encoding, consolidation, and retrieval of contextual memory: differential involvement of dorsal CA3 and CA1 hippocampal subregions. *Learn Mem* **12:** 375–382. doi:10.1101/lm.81905

Day M, Carr DB, Ulrich S, Ilijic E, Tkatch T, Surmeier DJ. 2005. Dendritic excitability of mouse frontal cortex pyramidal neurons is shaped by the interaction among HCN, Kir2, and Kleak channels. *J Neurosci* **25:** 8776–8787. doi:10.1523/JNEUROSCI.2650-05.2005

Deacon RM. 2006. Assessing nest building in mice. *Nat Protoc* **1:** 1117–1119. doi:10.1038/nprot2006.170

de Landeta AB, Pereyra M, Medina JH, Katche C. 2020. Anterior retrosplenial cortex is required for long-term object recognition memory. *Sci Rep* **10:** 4002. doi:10.1038/s41598-020-60937-z

Delotterie DF, Mathis C, Cassel JC, Rosenbrock H, Dorner-Ciossek C, Marti A. 2015. Touchscreen tasks in mice to demonstrate differences between hippocampal and striatal functions. *Neurobiol Learn Mem* **120:** 16–27. doi:10.1016/j.nlm.2015.02.007

Del Pino I, Rico B, Marin O. 2018. Neural circuit dysfunction in mouse models of neurodevelopmental disorders. *Curr Opin Neurobiol* **48:** 174–182. doi:10.1016/j.conb.2017.12.013

Fleischmann A, Hvalby O, Jensen V, Strekalova T, Zacher C, Layer LE, Kvello A, Reschke M, Spanagel R, Sprengel R, et al. 2003. Impaired long-term memory and NR2A-type NMDA receptor-dependent synaptic plasticity in mice lacking c-Fos in the CNS. *J Neurosci* **23:** 9116–9122. doi:10.1523/JNEUROSCI.23-27-09116.2003

Fordyce DE, Bhat RV, Baraban JM, Wehner JM. 1994. Genetic and activity-dependent regulation of zif268 expression: association with spatial learning. *Hippocampus* **4:** 559–568. doi:10.1002/hipo.450040505

Foss-Feig JH, Adkinson BD, Ji JL, Yang G, Srihari VH, McPartland JC, Krystal JH, Murray JD, Anticevic A. 2017. Searching for cross-diagnostic convergence: neural mechanisms governing excitation and inhibition balance in schizophrenia and autism spectrum disorders. *Biol Psychiatry* **81:** 848–861. doi:10.1016/j.biopsych.2017.03.005

Gall C, Murray K, Isackson PJ. 1991. Kainic acid-induced seizures stimulate increased expression of nerve growth factor mRNA in rat hippocampus. *Brain Res Mol Brain Res* **9:** 113–123. doi:10.1016/0169-328X(91)90136-L

Gerlai R. 1998. Contextual learning and cue association in fear conditioning in mice: a strain comparison and a lesion study. *Behav Brain Res* **95:** 191–203. doi:10.1016/S0166-4328(97)00144-7

Gerlai R. 2002. Hippocampal LTP and memory in mouse strains: is there evidence for a causal relationship? *Hippocampus* **12:** 657–666. doi:10.1002/hipo.10101

Guzowski JF, Setlow B, Wagner EK, McGaugh JL. 2001. Experience-dependent gene expression in the rat hippocampus after spatial learning: a comparison of the immediate-early genes Arc, c-fos, and zif268. *J Neurosci* **21:** 5089–5098. doi:10.1523/JNEUROSCI.21-14-05089.2001

Hardingham GE, Arnold FJ, Bading H. 2001. Nuclear calcium signaling controls CREB-mediated gene expression triggered by synaptic activity. *Nat Neurosci* **4:** 261–267. doi:10.1038/85109

Hasegawa Y, Mukai H, Asashima M, Hojo Y, Ikeda M, Komatsuzaki Y, Ooishi Y, Kawato S. 2014. Acute modulation of synaptic plasticity of pyramidal neurons by activin in adult hippocampus. *Front Neural Circuits* **8:** 56. doi:10.3389/fncir.2014.00056

Hawk JD, Bookout AL, Poplawski SG, Bridi M, Rao AJ, Sulewski ME, Kroener BT, Manglesdorf DJ, Abel T. 2012. NR4A nuclear receptors support memory enhancement by histone deacetylase inhibitors. *J Clin Invest* **122:** 3593–3602. doi:10.1172/JCI64145

Hemstedt TJ, Bengtson CP, Ramirez O, Oliveira AMM, Bading H. 2017. Reciprocal interaction of dendrite geometry and nuclear calcium-VEGFD signaling gates memory consolidation and extinction. *J Neurosci* **37:** 6946–6955. doi:10.1523/JNEUROSCI.2345-16.2017

Holmes A, Wrenn CC, Harris AP, Thayer KE, Crawley JN. 2002. Behavioral profiles of inbred strains on novel olfactory, spatial and emotional tests for reference memory in mice. *Genes Brain Behav* **1:** 55–69. doi:10.1046/j.1601-1848.2001.00005.x

Horner AE, Heath CJ, Hvoslef-Eide M, Kent BA, Kim CH, Nilsson SR, Alsio J, Oomen CA, Holmes A, Saksida LM, et al. 2013. The touchscreen operant platform for testing learning and memory in rats and mice. *Nat Protoc* **8:** 1961–1984. doi:10.1038/nprot.2013.122

Hwang YK, Song JC, Han SH, Cho J, Smith DR, Gallagher M, Han JS. 2010. Differences in hippocampal CREB phosphorylation in trace fear conditioning of two inbred mouse strains. *Brain Res* **1345:** 156–163. doi:10.1016/j.brainres.2010.05.048

Iwahori Y, Saito H, Torii K, Nishiyama N. 1997. Activin exerts a neurotrophic effect on cultured hippocampal neurons. *Brain Res* **760:** 52–58. doi:10.1016/S0006-8993(97)00275-8

Jones MW, Peckham HM, Errington ML, Bliss TV, Routtenberg A. 2001. Synaptic plasticity in the hippocampus of awake C57BL/6 and DBA/2 mice: interstrain differences and parallels with behavior. *Hippocampus* **11:** 391–396. doi:10.1002/hipo.1053

Kase D, Imoto K. 2012. The role of HCN channels on membrane excitability in the nervous system. *J Signal Transduct* **2012:** 619747. doi:10.1155/2012/619747

Kesner RP. 2009. The posterior parietal cortex and long-term memory representation of spatial information. *Neurobiol Learn Mem* **91:** 197–206. doi:10.1016/j.nlm.2008.09.004

Kilkenny C, Browne WJ, Cuthill IC, Emerson M, Altman DG. 2010. Improving bioscience research reporting: the ARRIVE guidelines for reporting animal research. *PLoS Biol* **8:** e1000412. doi:10.1371/journal.pbio.1000412

Kochli DE, Thompson EC, Fricke EA, Postle AF, Quinn JJ. 2015. The amygdala is critical for trace, delay, and contextual fear conditioning. *Learn Mem* **22:** 92–100. doi:10.1101/lm.034918.114

Koppe G, Mallien AS, Berger S, Bartsch D, Gass P, Vollmayr B, Durstewitz D. 2017. CACNA1C gene regulates behavioral strategies in operant rule learning. *PLoS Biol* **15:** e2000936. doi:10.1371/journal.pbio.2000936

Krieglstein K, Zheng F, Unsicker K, Alzheimer C. 2011. More than being protective: functional roles for TGF-β/activin signaling pathways at

central synapses. *Trends Neurosci* **34:** 421–429. doi:10.1016/j.tins.2011.06.002

Lee J, Chung C, Ha S, Lee D, Kim DY, Kim H, Kim E. 2015. Shank3-mutant mice lacking exon 9 show altered excitation/inhibition balance, enhanced rearing, and spatial memory deficit. *Front Cell Neurosci* **9:** 94. doi:10.3389/fncel.2015.00094

Le Gal La Salle G, Naquet R. 1990. Audiogenic seizures evoked in DBA/2 mice inducec-fos oncogene expression into subcortical auditory nuclei. *Brain Res* **518:** 308–312. doi:10.1016/0006-8993(90)90988-N

Legon W, Punzell S, Dowlati E, Adams SE, Stiles AB, Moran RJ. 2016. Altered prefrontal excitation/inhibition balance and prefrontal output: markers of aging in human memory networks. *Cereb Cortex* **26:** 4315–4326. doi:10.1093/cercor/bhv200

Lenselink AM, Rotaru DC, Li KW, van Nierop P, Rao-Ruiz P, Loos M, van der Schors R, Gouwenberg Y, Wortel J, Mansvelder HD, et al. 2015. Strain differences in presynaptic function: proteomics, ultrastructure, and physiology of hippocampal synapses in DBA/2J and C57Bl/6J mice. *J Biol Chem* **290:** 15635–15645. doi:10.1074/jbc.M114.628776

Lin Y, Bloodgood BL, Hauser JL, Lapan AD, Koon AC, Kim TK, Hu LS, Malik AN, Greenberg ME. 2008. Activity-dependent regulation of inhibitory synapse development by Npas4. *Nature* **455:** 1198–1204. doi:10.1038/nature07319

Liu X, Muller RU, Huang LT, Kubie JL, Rotenberg A, Rivard B, Cilio MR, Holmes GL. 2003. Seizure-induced changes in place cell physiology: relationship to spatial memory. *J Neurosci* **23:** 11505–11515. doi:10.1523/JNEUROSCI.23-37-11505.2003

Logue SF, Paylor R, Wehner JM. 1997. Hippocampal lesions cause learning deficits in inbred mice in the Morris water maze and conditioned-fear task. *Behav Neurosci* **111:** 104–113. doi:10.1037/0735-7044.111.1.104

Lucas EK, Clem RL. 2018. GABAergic interneurons: the orchestra or the conductor in fear learning and memory? *Brain Res Bull* **141:** 13–19. doi:10.1016/j.brainresbull.2017.11.016

Mallien AS, Palme R, Richetto J, Muzzillo C, Richter SH, Vogt MA, Inta D, Riva MA, Vollmayr B, Gass P. 2016. Daily exposure to a touchscreen-paradigm and associated food restriction evokes an increase in adrenocortical and neural activity in mice. *Horm Behav* **81:** 97–105. doi:10.1016/j.yhbeh.2016.03.009

Matsuyama S, Namgung U, Routtenberg A. 1997. Long-term potentiation persistence greater in C57BL/6 than DBA/2 mice: predicted on basis of protein kinase C levels and learning performance. *Brain Res* **763:** 127–130. doi:10.1016/S0006-8993(97)00444-7

McAvoy K, Besnard A, Sahay A. 2015. Adult hippocampal neurogenesis and pattern separation in DG: a role for feedback inhibition in modulating sparseness to govern population-based coding. *Front Syst Neurosci* **9:** 120. doi:10.3389/fnsys.2015.00120

McLin JP, Steward O. 2006. Comparison of seizure phenotype and neurodegeneration induced by systemic kainic acid in inbred, outbred, and hybrid mouse strains. *Eur J Neurosci* **24:** 2191–2202. doi:10.1111/j.1460-9568.2006.05111.x

McNulty SE, Barrett RM, Vogel-Ciernia A, Malvaez M, Hernandez N, Davatolhagh MF, Matheos DP, Schiffman A, Wood MA. 2012. Differential roles for Nr4a1 and Nr4a2 in object location vs. object recognition long-term memory. *Learn Mem* **19:** 588–592. doi:10.1101/lm.026385.112

Misiewicz Z, Iurato S, Kulesskaya N, Salminen L, Rodrigues L, Maccarrone G, Martins J, Czamara D, Laine MA, Sokolowska E, et al. 2019. Multi-omics analysis identifies mitochondrial pathways associated with anxiety-related behavior. *PLoS Genet* **15:** e1008358. doi:10.1371/journal.pgen.1008358

Mozhui K, Karlsson RM, Kash TL, Ihne J, Norcross M, Patel S, Farrell MR, Hill EE, Graybeal C, Martin KP, et al. 2010. Strain differences in stress responsivity are associated with divergent amygdala gene expression and glutamate-mediated neuronal excitability. *J Neurosci* **30:** 5357–5367. doi:10.1523/JNEUROSCI.5017-09.2010

Mulisch M, Welsch U. 2010. *Romeis-Mikroskopische Technik*. Springer Spektrum.

Muller MR, Zheng F, Werner S, Alzheimer C. 2006. Transgenic mice expressing dominant-negative activin receptor IB in forebrain neurons reveal novel functions of activin at glutamatergic synapses. *J Biol Chem* **281:** 29076–29084. doi:10.1074/jbc.M604959200

Nadel L. 1968. Dorsal and ventral hippocampal lesions and behavior. *Physiol Behav* **3:** 891–900. doi:10.1016/0031-9384(68)90174-1

Nguyen PV, Abel T, Kandel ER, Bourtchouladze R. 2000a. Strain-dependent differences in LTP and hippocampus-dependent memory in inbred mice. *Learn Mem* **7:** 170–179. doi:10.1101/lm.7.3.170

Nguyen PV, Duffy SN, Young JZ. 2000b. Differential maintenance and frequency-dependent tuning of LTP at hippocampal synapses of specific strains of inbred mice. *J Neurophysiol* **84:** 2484–2493. doi:10.1152/jn.2000.84.5.2484

Oh MM, Simkin D, Disterhoft JF. 2016. Intrinsic hippocampal excitability changes of opposite signs and different origins in CA1 and CA3

pyramidal neurons underlie aging-related cognitive deficits. *Front Syst Neurosci* **10:** 52.

Owen EH, Logue SF, Rasmussen DL, Wehner JM. 1997. Assessment of learning by the Morris water task and fear conditioning in inbred mouse strains and F1 hybrids: implications of genetic background for single gene mutations and quantitative trait loci analyses. *Neuroscience* **80:** 1087–1099. doi:10.1016/S0306-4522(97)00165-6

Passino E, Middei S, Restivo L, Bertaina-Anglade V, Ammassari-Teule M. 2002. Genetic approach to variability of memory systems: analysis of place vs. response learning and fos-related expression in hippocampal and striatal areas of C57BL/6 and DBA/2 mice. *Hippocampus* **12:** 63–75. doi:10.1002/hipo.10007

Paylor R, Baskall L, Wehner JM. 1993. Behavioral dissociations between C57BL/6 and DBA/2 mice on learning and memory tasks: a hippocampal-dysfunction hypothesis. *Psychobiology* **21:** 11–26.

Paylor R, Tracy R, Wehner J, Rudy JW. 1994. DBA/2 and C57BL/6 mice differ in contextual fear but not auditory fear conditioning. *Behav Neurosci* **108:** 810–817. doi:10.1037/0735-7044.108.4.810

Podhorna J, Brown RE. 2002. Strain differences in activity and emotionality do not account for differences in learning and memory performance between C57BL/6 and DBA/2 mice. *Genes Brain Behav* **1:** 96–110. doi:10.1034/j.1601-183X.2002.10205.x

Poolos NP, Migliore M, Johnston D. 2002. Pharmacological upregulation of h-channels reduces the excitability of pyramidal neuron dendrites. *Nat Neurosci* **5:** 767–774. doi:10.1038/nn891

Pruunsild P, Sepp M, Orav E, Koppel I, Timmusk T. 2011. Identification of cis-elements and transcription factors regulating neuronal activity-dependent transcription of human BDNF gene. *J Neurosci* **31:** 3295–3308. doi:10.1523/JNEUROSCI.4540-10.2011

Ramamoorthi K, Fropf R, Belfort GM, Fitzmaurice HL, McKinney RM, Neve RL, Otto T, Lin Y. 2011. Npas4 regulates a transcriptional program in CA3 required for contextual memory formation. *Science* **334:** 1669–1675. doi:10.1126/science.1208049

Rebecca Glatt A, St John SJ, Lu L, Boughter JD Jr. 2016. Temporal and qualitative dynamics of conditioned taste aversions in C57BL/6J and DBA/2J mice self-administering LiCl. *Physiol Behav* **153:** 97–108. doi:10.1016/j.physbeh.2015.10.033

Reichstein D, Ren L, Filippopoulos T, Mittag T, Danias J. 2007. Apoptotic retinal ganglion cell death in the DBA/2 mouse model of glaucoma. *Exp Eye Res* **84:** 13–21. doi:10.1016/j.exer.2006.08.009

Restivo L, Roman FS, Ammassari-Teule M, Marchetti E. 2006. Simultaneous olfactory discrimination elicits a strain-specific increase in dendritic spines in the hippocampus of inbred mice. *Hippocampus* **16:** 472–479. doi:10.1002/hipo.20174

Richter SH, Vogel AS, Ueltzhoffer K, Muzzillo C, Vogt MA, Lankisch K, Armbruster-Genc DJ, Riva MA, Fiebach CJ, Gass P, et al. 2014. Touchscreen-paradigm for mice reveals cross-species evidence for an antagonistic relationship of cognitive flexibility and stability. *Front Behav Neurosci* **8:** 154. doi:10.3389/fnbeh.2014.00154

Robitsek J, Ratner MH, Stewart T, Eichenbaum H, Farb DH. 2015. Combined administration of levetiracetam and valproic acid attenuates age-related hyperactivity of CA3 place cells, reduces place field area, and increases spatial information content in aged rat hippocampus. *Hippocampus* **25:** 1541–1555. doi:10.1002/hipo.22474

Rossi-Arnaud C, Fagioli S, Ammassari-Teule M. 1991. Spatial learning in two inbred strains of mice: genotype-dependent effect of amygdaloid and hippocampal lesions. *Behav Brain Res* **45:** 9–16. doi:10.1016/S0166-4328(05)80175-5

Roux L, Buzsaki G. 2015. Tasks for inhibitory interneurons in intact brain circuits. *Neuropharmacology* **88:** 10–23. doi:10.1016/j.neuropharm.2014.09.011

Satoh Y, Endo S, Ikeda T, Yamada K, Ito M, Kuroki M, Hiramoto T, Imamura O, Kobayashi Y, Watanabe Y, et al. 2007. Extracellular signal-regulated kinase 2 (ERK2) knockdown mice show deficits in long-term memory; ERK2 has a specific function in learning and memory. *J Neurosci* **27:** 10765–10776. doi:10.1523/JNEUROSCI.0117-07.2007

Schimanski LA, Nguyen PV. 2005. Impaired fear memories are correlated with subregion-specific deficits in hippocampal and amygdalar LTP. *Behav Neurosci* **119:** 38–54. doi:10.1037/0735-7044.119.1.38

Schreiber RA, Graham JM Jr. 1976. Audiogenic priming in DBA/2J and C57BL/6J mice: interactions among age, prime-to-test interval and index of seizure. *Dev Psychobiol* **9:** 57–66. doi:10.1002/dev.420090109

Schwegler H, Crusio WE, Brust I. 1990. Hippocampal mossy fibers and radial-maze learning in the mouse: a correlation with spatial working memory but not with non-spatial reference memory. *Neuroscience* **34:** 293–298. doi:10.1016/0306-4522(90)90139-U

Sekiguchi M, Hayashi F, Tsuchida K, Inokuchi K. 2009. Neuron type-selective effects of activin on development of the hippocampus. *Neurosci Lett* **452:** 232–237. doi:10.1016/j.neulet.2009.01.074

Seo MS, Lee B, Kang KK, Sung SE, Choi JH, Lee SJ, Kim YI, Jung YS, Kim UK, Kim KS. 2021. Phenotype of the aging-dependent spontaneous

onset of hearing loss in DBA/2 mice. *Vet Sci* **8:** 49. doi:10.3390/vetsci8030049

Sim S, Antolin S, Lin CW, Lin Y, Lois C. 2013. Increased cell-intrinsic excitability induces synaptic changes in new neurons in the adult dentate gyrus that require Npas4. *J Neurosci* **33:** 7928–7940. doi:10.1523/JNEUROSCI.1571-12.2013

Spiegel I, Mardinly AR, Gabel HW, Bazinet JE, Couch CH, Tzeng CP, Harmin DA, Greenberg ME. 2014. Npas4 regulates excitatory-inhibitory balance within neural circuits through cell-type-specific gene programs. *Cell* **157:** 1216–1229. doi:10.1016/j.cell.2014.03.058

Sun X, Lin Y. 2016. Npas4: linking neuronal activity to memory. *Trends Neurosci* **39:** 264–275. doi:10.1016/j.tins.2016.02.003

Sung JY, Goo JS, Lee DE, Jin DQ, Bizon JL, Gallagher M, Han JS. 2008. Learning strategy selection in the water maze and hippocampal CREB phosphorylation differ in two inbred strains of mice. *Learn Mem* **15:** 183–188. doi:10.1101/lm.783108

Talpos JC, Winters BD, Dias R, Saksida LM, Bussey TJ. 2009. A novel touchscreen-automated paired-associate learning (PAL) task sensitive to pharmacological manipulation of the hippocampus: a translational rodent model of cognitive impairments in neurodegenerative disease. *Psychopharmacology (Berl)* **205:** 157–168. doi:10.1007/s00213-009-1526-3

Tan HO, Reid CA, Single FN, Davies PJ, Chiu C, Murphy S, Clarke AL, Dibbens L, Krestel H, Mulley JC, et al. 2007. Reduced cortical inhibition in a mouse model of familial childhood absence epilepsy. *Proc Natl Acad Sci* **104:** 17536–17541. doi:10.1073/pnas.0708440104

Tan HO, Reid CA, Chiu C, Jones MV, Petrou S. 2008. Increased thalamic inhibition in the absence seizure prone DBA/2J mouse. *Epilepsia* **49:** 921–925. doi:10.1111/j.1528-1167.2008.01536.x

Thinus-Blanc C, Save E, Rossi-Arnaud C, Tozzi A, Ammassari-Teule M. 1996. The differences shown by C57BL/6 and DBA/2 inbred mice in detecting spatial novelty are subserved by a different hippocampal and parietal cortex interplay. *Behav Brain Res* **80:** 33–40. doi:10.1016/0166-4328(96)00016-2

Tipps ME, Raybuck JD, Buck KJ, Lattal KM. 2014. Delay and trace fear conditioning in C57BL/6 and DBA/2 mice: issues of measurement and performance. *Learn Mem* **21:** 380–393. doi:10.1101/lm.035261.114

Tsien JZ, Huerta PT, Tonegawa S. 1996. The essential role of hippocampal CA1 NMDA receptor-dependent synaptic plasticity in spatial memory. *Cell* **87:** 1327–1338. doi:10.1016/S0092-8674(00)81827-9

Tzingounis AV, Nicoll RA. 2006. Arc/Arg3.1: linking gene expression to synaptic plasticity and memory. *Neuron* **52:** 403–407. doi:10.1016/j.neuron.2006.10.016

Upchurch M, Wehner JM. 1988. Differences between inbred strains of mice in Morris water maze performance. *Behav Genet* **18:** 55–68. doi:10.1007/BF01067075

Valero M, Averkin RG, Fernandez-Lamo I, Aguilar J, Lopez-Pigozzi D, Brotons-Mas JR, Cid E, Tamas G, Menendez de la Prida L. 2017. Mechanisms for selective single-cell reactivation during offline sharp-wave ripples and their distortion by fast ripples. *Neuron* **94:** 1234–1247 e1237. doi:10.1016/j.neuron.2017.05.032

Volpe BT, Davis HP, Towle A, Dunlap WP. 1992. Loss of hippocampal CA1 pyramidal neurons correlates with memory impairment in rats with ischemic or neurotoxin lesions. *Behav Neurosci* **106:** 457–464. doi:10.1037/0735-7044.106.3.457

Wehner JM, Sleight S, Upchurch M. 1990. Hippocampal protein kinase C activity is reduced in poor spatial learners. *Brain Res* **523:** 181–187. doi:10.1016/0006-8993(90)91485-Y

Weng FJ, Garcia RI, Lutzu S, Alvina K, Zhang Y, Dushko M, Ku T, Zemoura K, Rich D, Garcia-Dominguez D, et al. 2018. Npas4 is a critical regulator of learning-induced plasticity at mossy fiber-CA3 synapses during contextual memory formation. *Neuron* **97:** 1137–1152 e1135. doi:10.1016/j.neuron.2018.01.026

Willott JF, Lu SM. 1980. Midbrain pathways of audiogenic seizures in DBA/2 mice. *Exp Neurol* **70:** 288–299. doi:10.1016/0014-4886(80)90028-X

Wisden W, Seeburg PH. 1993. A complex mosaic of high-affinity kainate receptors in rat brain. *J Neurosci* **13:** 3582–3598. doi:10.1523/JNEUROSCI.13-08-03582.1993

Youn J, Ellenbroek BA, van Eck I, Roubos S, Verhage M, Stiedl O. 2012. Finding the right motivation: genotype-dependent differences in effective reinforcements for spatial learning. *Behav Brain Res* **226:** 397–403. doi:10.1016/j.bbr.2011.09.034

Young EA, Owen EH, Meiri KF, Wehner JM. 2000. Alterations in hippocampal GAP-43 phosphorylation and protein level following contextual fear conditioning. *Brain Res* **860:** 95–103. doi:10.1016/S0006-8993(00)02021-7

Zhang SJ, Steijaert MN, Lau D, Schutz G, Delucinge-Vivier C, Descombes P, Bading H. 2007. Decoding NMDA receptor signaling: identification of genomic programs specifying neuronal survival and death. *Neuron* **53:** 549–562. doi:10.1016/j.neuron.2007.01.025

Zhang SJ, Zou M, Lu L, Lau D, Ditzel DA, Delucinge-Vivier C, Aso Y, Descombes P, Bading H. 2009. Nuclear calcium signaling controls expression of a large gene pool: identification of a gene program for acquired neuroprotection induced by synaptic activity. *PLoS Genet* **5:** e1000604. doi:10.1371/journal.pgen.1000604